

1 **Intercomparison of Aerosol Optical Depths from four reanalyses and their**
2 **multi-reanalysis-consensus**

3
4 Peng Xian¹, Jeffrey S. Reid¹, Melanie Ades², Angela Benedetti², Peter R. Colarco³, Arlindo da
5 Silva³, Tom F. Eck^{3,4}, Johannes Flemming², Edward J. Hyer¹, Zak Kipling², Samuel Rémy⁵,
6 Tsuyoshi Thomas Sekiyama⁶, Taichu Tanaka⁷, Keiya Yumimoto⁸ and Jianglong Zhang⁹

7
8 ¹Naval Research Laboratory, Monterey, CA, USA.

9 ²European Centre for Medium-Range Weather Forecasts, Reading, UK.

10 ³NASA Goddard Space Flight Center, Greenbelt, MD, USA.

11 ⁴University of Maryland Baltimore County, Baltimore, MD, USA

12 ⁵HYGEOS, Lille, France

13 ⁶Meteorological Research Institute, Japan Meteorological Agency, Tsukuba, Japan

14 ⁷Information Infrastructure Department, Japan Meteorological Agency, Tokyo, Japan

15 ⁸Research Institute for Applied Mechanics, Kyushu University, Kasuga, Japan

16 ⁹Department of Atmospheric Sciences, University of North Dakota, Grand Forks, ND

17
18 Corresponding author: Peng Xian (peng.xian@nrlmry.navy.mil)

19
20
21 **Key Points:**

- 22 1. Four global aerosol reanalyses are intercompared and verified with observations for their
23 skill in simulating aerosol optical depth.
24 2. The study identifies the strength of each reanalysis and the regions where there are
25 notable differences and challenges.
26 3. The multi-reanalysis-consensus, based on the four reanalyses, consistently ranks as one
27 of the best regionally and globally.

28
29 **Abstract**

30 The emergence of aerosol reanalyses in recent years has facilitated a comprehensive and
31 systematic evaluation of Aerosol Optical Depth (AOD) trends and attribution over multi-decadal
32 timescales. Notable **multiyear** aerosol reanalyses currently available include NAAPS-RA from the
33 U.S. Naval Research Laboratory; the NASA MERRA-2; JRAero from the Japan Meteorological
34 Agency (JMA); and CAMSRA from Copernicus/ECMWF. These aerosol reanalyses are based on
35 differing underlying meteorology models, representations of aerosol processes, and data
36 assimilation methods and treatment of AOD observations. This study presents the basic
37 verification characteristics of these four reanalyses versus both AERONET and MODIS retrievals
38 in monthly AOD properties and identifies the strength of each reanalysis and the regions where
39 **diversitydivergence** and challenges are prominent. Regions with high pollution and often mixed
40 fine-coarse mode aerosol environments such as South Asia, East Asia, Southeast Asia, and the

41 Maritime Continent pose significant challenges, as indicated by higher monthly AOD root mean
42 square error. Moreover, regions that are distant from major aerosol source areas, including the
43 polar regions, and remote oceans, exhibit large relative differences in speciated AODs and fine-
44 mode vs coarse-mode AODs among the four reanalyses. To ensure consistency across the globe,
45 a multi-reanalysis-consensus (MRC, i.e. ensemble mean) approach was developed similar to the
46 International Cooperative for Aerosol Prediction Multi-Model Ensemble (ICAP-MME). Like the
47 ICAP-MME, while the MRC does not consistently rank first among the reanalyses for individual
48 regions, it performs well by ranking first or second globally in AOD correlation and RMSE,
49 making it a suitable candidate for climate studies that require robust and consistent assessments.

50

51 Keywords: Aerosol, Reanalysis, Aerosol Optical Depth, intercomparison, ICAP-MME

52

53 Short Summary

54 The study compares and evaluates monthly aerosol optical depth of four reanalyses (RA) and their
55 consensus- (i.e. ensemble mean). The basic verification characteristics of these RA versus both
56 AERONET and MODIS retrievals are presented. The study discusses the strength of each RA and
57 identifies regions where diversitydivergence and challenges are prominent. The RA consensus
58 usually performs very well on a global scale in terms of how well it matches the observational
59 data, making it a good choice for various applications.

60

61 1. Introduction

62 In recent years, global aerosol reanalyses have been developed by major operational and research
63 centers, owing to the availability of long-record satellite remote sensing aerosol products and
64 advancements in aerosol data assimilation and modeling. These reanalyses are based on their
65 operational counterparts that are included in the "Core Four" members of the International
66 Cooperative for Aerosol Prediction Multi Model Ensemble (ICAP-MME C4C; Sessions et al.,
67 ~~2016~~2015; Xian et al., 2019; Reid et al., 2022). The reanalyses include the Copernicus Atmosphere
68 Monitoring Service ReAnalysis (CAMSR; Inness et al., 2019) produced by the European Centre
69 for Medium-Range Weather Forecasts (ECMWF); the Japanese Reanalysis for Aerosol (JRAero)
70 (Yumimoto et al., 2017) developed by the Japan Meteorological Agency (JMA); the NASA
71 Modern-Era Retrospective Analysis for Research and Applications, version 2 (MERRA-2;
72 Randles et al., 2017); and the Navy Aerosol Analysis and Prediction System reanalysis (NAAPS-
73 RA; Lynch et al., 2016) developed by the U.S. Naval Research Laboratory (NRL).

74 The aerosol reanalyses are similar to their operational counterparts and characterized by a high
75 degree of independence in their underlying meteorology, aerosol sources, sinks, microphysics, and
76 chemistry, as well as in their assimilation methods for aerosol optical depth (AOD) observations.
77 A summary of the configurations of these four reanalyses is presented in Table 1 for general
78 features and Table 2 for microphysical and optical treatments of different aerosol species. Notably,
79 the use of operational Terra and Aqua Moderate Resolution Imaging Spectrometer data (MODIS
80 Dark Target and Deep Blue; Levy et al., 2013; Hsu et al., 2013) is consistent across these
81 reanalyses, although preprocessing treatments vary. These treatments include quality control, bias
82 correction, and aggregation and sampling. Additionally, several other products, such as
83 MultiAngle Imaging Spectroradiometer (MISR; Kahn et al., 2010), Advanced Very High
84 Resolution Radiometer (AVHRR; e.g., Ignatov et al., 2002), and ~~Polar Multi-Sensor Aerosol~~
85 ~~product (PMAp; Grzegorski~~ Advanced Along-Track Scanning Radiometer (AATSR, Popp et al.,
86 2022),2016 are assimilated into some of these reanalyses, although these additional remote
87 sensing data probably have only a small impact during the MODIS era, as their data volume is
88 small compared to MODIS. Therefore, between their underlying meteorology, physics, and data
89 assimilation these reanalyses are characterized by a high degree of independence overall.

90 Like atmospheric reanalysis products, aerosol reanalysis products, whether used individually or in
91 combination, have been employed for diverse applications. They provide comprehensive aerosol
92 climatology and statistics to aid in understanding aerosol conditions across various regions and the
93 world (e.g., Reid et al., 2012; Xian et al., 2020; Nignombam et al., 2021; Ohno et al., 2022; Rubin
94 et al., 2023). They are widely used to address a multitude of scientific inquiries in the fields of
95 aerosol radiative forcing (e.g., Randles et al., 2017; Markowicz et al., 2017; 2021a,b; Ohno et al.,
96 2022; Zhang et al., 2023), aerosol-cloud interaction (e.g., McCoy et al., 2017; Ross et al., 2018;
97 Eck et al., 2018), aerosol-cryosphere interaction (e.g., Khan et al., 2018, 2019; 2020;
98 Roychoudhury et al., 2022), air quality and its impact on health (e.g., Tong et al., 2023; Cui et al.,
99 2022; Jenwitheesuk et al., 2022; Lacima et al., 2022), biogeochemical cycles (e.g., Rahav et al.,
100 2020; Borchardt et al., 2019; Mescioglu et al., 2019), among others. These reanalyses have been
101 rigorously evaluated by the developing centers and various studies from different perspectives,
102 including AOD and other aerosol optical properties, mass concentrations, and vertical distribution
103 profiles. However, to date, no intercomparison among the four reanalyses has been conducted.

Formatted: English (United Kingdom)

Formatted: English (United Kingdom)

104 This study presents an intercomparison of the four available global aerosol reanalyses to evaluate
105 their skill in simulating monthly average AOD. Additionally, this study includes the development
106 of a Multi Reanalysis Consensus (MRC) product using a multi-model-consensus approach, similar
107 to the ICAP Multi Model Ensemble (ICAP-MME; Sessions et al., 2015; Xian et al., 2019). The
108 MRC is ~~a consensus~~ an ensemble mean (i.e., mathematical average) of the four individual
109 reanalyses, with a spatial resolution of $1^\circ \times 1^\circ$ latitude/longitude and monthly temporal resolution.
110 The study provides speciated AODs, fine-mode (FM), coarse-mode (CM) and total AODs at 550
111 nm for the period of 2003-2019 from three reanalyses, and all four reanalyses are available for the
112 time period of 2011-2019. In addition, a companion study focuses on global and regional AOD
113 trends derived from these reanalyses. The validation of AODs from the MRC, and the four
114 component members, is performed using ground-based AEROSol Robotic NETwork (AERONET;
115 Holben et al., 1998) observations, with MODIS AOD for spatial distribution evaluation. The
116 validation results, as well as the AOD climatology and diversity/divergence of the reanalyses, are
117 presented in Section 3. The study concludes with a summary of the findings in Section 4.

118

119 2. Data and Methods

120 This study intercompares the monthly average modal (total, FM, and CM) and speciated AOD
121 products from four aerosol reanalyses (RA) and their consensus, and evaluates the RA AODs with
122 AERONET and the combined MODIS Dark Target/Deep Blue retrievals (Levy et al., 2013; Hsu
123 et al., 2013).

124 2.1 Individual product lines

125 Descriptions of the four reanalysis datasets, including CAMSRA, JRAero, MERRA-2, and
126 NAAPS-RA v1, are provided in this section. Table 1 provides a summary of the ~~features of the~~
127 ~~four reanalyses and the MRC used in this study.~~ basic features of the four reanalyses and the MRC
128 used in this study. Table 2 offers a summary of the parameters employed to depict the
129 microphysical and optical properties of aerosol species from these reanalyses. Furthermore, Table
130 3 samples hygroscopic enhancement factor values that influence optical property calculations due
131 to the hygroscopic growth of particles at various relative humidity levels. In addition to utilizing
132 different meteorological data, aerosol source data, AOD observations, and constructing aerosol
133 species, notable differences exist even among similar species regarding treatments related to
134 aerosol microphysics, optical properties, and water uptake ability for hydrophilic species.

135 2.1.1 CAMSRA

136 The Copernicus Atmosphere Monitoring Service (CAMS) Reanalysis (CAMSRA, Inness et al.,
137 2019) is run at the European Centre for Medium-Range Weather Forecasts (ECMWF) and is a
138 global reanalysis of atmospheric composition species, including aerosols. It builds on the
139 previous reanalyses of the MACC project (Inness et al., 2013) and the CAMS interim reanalysis
140 (Flemming et al., 2017). The CAMSRA is publicly available for the years 2003 to 2022 and is
141 being continuously updated for future years.

142 The CAMSRA is based on the Integrated Forecasting System (IFS) used by ECMWF for
143 numerical weather prediction and meteorological reanalysis. Two additional modules are
144 incorporated into the IFS for the CAMSRA, one to calculate the processes and reactions of the
145 chemical species and one to represent the prognostic aerosol species. The aerosol scheme
146 includes prescribed and online emissions, dry and wet deposition, production of sulfate from a
147 gas-phase sulfur dioxide precursor, and the aging of hydrophobic organic matter (OM) and black
148 carbon (BC) to hydrophilic. The prescribed anthropogenic emissions come from the MACCity
149 inventory (Granier et al., 2011) and the biomass burning (BB) emissions from the Global Fire
150 Assimilation System, version 1.2 (GFASv1.2) (Kaiser et al., 2012). GFASv1.2 is a separate
151 system to the IFS that uses satellite retrievals of fire radiative power to produce the BB emissions
152 that are then input as fixed emissions to the aerosol scheme. The transport of the aerosol species
153 by advection, convection and diffusion is calculated using the meteorological component of the
154 IFS and the wind fields from the meteorology are also used as parameters to estimate the online
155 sea salt (Monahan et al., 1986) and dust (Ginoux et al., 2001) surface emissions. One key
156 difference between the CAMSRA set up of the IFS and that used for numerical weather
157 prediction, is that for the CAMSRA the radiative impact of aerosol particles and ozone on
158 meteorology is also accounted for.

159 The observations used in the CAMSRA for aerosols are of total AOD at 550nm. These come
160 from MODIS collection 6 satellite retrievals for the entire period covered by CAMSRA and from
161 the Advanced Along-Track Scanning Radiometer for the period 2003-2012. These AOD
162 observations are simultaneously assimilated with trace gas and meteorological observations
163 using the 4D variational data assimilation system of the IFS with a 12-hour assimilation window.
164 The products available from the CAMSRA include speciated AODs at a 3-hour temporal and
165 approximately 0.7 degrees spatial resolution, whereas monthly mean AODs at 550nm were used
166 in this study.

167 2.1.2 JRAero

168 The Japanese Reanalysis for Aerosol (JRAero) was developed by the Meteorological Research
169 Institute (MRI) of the Japan Meteorological Agency and Kyushu University using the global
170 aerosol transport model MASINGAR Mk-2 (Yukimoto et al., 2012) and a two-dimensional
171 variational (2D-Var) data assimilation method. The model uses the MRI-AGCM3 atmospheric
172 general circulation model, and considers major tropospheric aerosol components, including black
173 carbon (BC), organic carbon (OC), mineral dust, sea salt, and sulfate aerosols, and their precursors.

174 JRAero assimilates global AOD from a bias-corrected MODIS Level 3 AOD product provided by
175 the US Naval Research Laboratory (NRL) and the University of North Dakota
176 (<http://doi.org/10.5067/MODIS/MCDAODHD.NRT.061>) every 6 hours. Anthropogenic and
177 biomass burning emissions were estimated using the MACCity (MACC/CityZEN EU projects)
178 emission inventory (http://accent.aero.jussieu.fr/MACC_metadata.php) and the Global Fire
179 Assimilation System (GFAS) dataset ([http://www.gmes-
atmosphere.eu/about/project_structure/input_data/d_fire](http://www.gmes-atmosphere.eu/about/project_structure/input_data/d_fire)). The reanalysis has a resolution of

181 TL159 (about $1.1^\circ \times 1.1^\circ$) with 48 vertical layers from the ground to 0.4 hPa. Validation results
182 and additional information can be found in Yumimoto et al. (2017).

183 2.1.3 MERRA-2

184 The NASA Modern-Era Retrospective Analysis for Research and Applications, version 2
185 (MERRA-2, Gelaro et al. 2017) is an atmospheric and aerosol reanalysis produced with the
186 NASA Goddard Earth Observing System (GEOS) Earth system model. Aerosol data assimilation
187 brings in data from the MODIS and MISR satellite sensors (after 2000) and includes AERONET
188 ground-based sun photometer observations (through 2014). The Goddard Chemistry, Aerosol,
189 Radiation, and Transport model (GOCART; Chin et al. 2000; Colarco et al. 2010) is run online
190 and radiatively coupled in the MERRA-2 system, and provides simulations of dust, sea salt,
191 sulfate, and black and organic carbon aerosol species.

192 Black and organic carbon are each partitioned into hydrophobic and hydrophilic modes, and a
193 single bulk sulfate aerosol species is carried. Dust and sea salt are partitioned into five non-
194 interacting size bins, with dust emissions based on the model 10-m wind speed and a topographic
195 source function following Ginoux et al. (2001), and sea salt emissions driven by the surface wind
196 friction speed modified from Gong (2003) and with a sea-surface temperature adjustment based
197 on Jaeglé et al. (2011). Explosive volcanic sulfur emissions are included through 2010 based on
198 Diehl et al. (2012), with a repeating annual cycle of degassing volcanic emissions subsequent.
199 Other emissions are as summarized in Table 1.

200 The analysis of AOD is performed on quality-controlled MODIS, MISR, and AERONET data as
201 described in Randles et al. (2017) and Buchard et al. (2015). The AOD analysis is performed by
202 means of analysis splitting, where first a 2-D analysis of AOD is performed using error
203 covariances derived from innovation data. Three-dimensional analysis increments for aerosol
204 mass concentration are then computed using the Local Displacement Ensemble (LDE)
205 methodology, which accommodates misplacement of the aerosol plumes due to source or
206 transport issues. The ensemble perturbations are generated at the full model resolution, without
207 the need for multiple model runs. Online quality control is performed as in Dee et al. (2001),
208 with observation and background errors estimated as in Dee and da Silva (1999). Randles et al.
209 (2017) and Buchard et al. (2017) describe the overall methodology and validation of the
210 MERRA-2 AOD reanalysis. For this study, monthly mean speciated AODs and total AOD at 550
211 nm with 0.5 degree latitude and 0.625 degree longitude spatial resolution were used.

212 2.1.4 NAAPS-RA v1

213 The Navy Aerosol Analysis and Prediction System (NAAPS, Lynch et al., 2016) is a global offline
214 chemical transport model developed at the U.S. Naval Research Laboratory. NAAPS simulates the
215 life cycles of aerosol particles and their gaseous precursors. The particle species include
216 anthropogenic and biogenic fine (ABF, a mix of sulfate, organic aerosols and BC from non-BB
217 sources), BB smoke, aeolian dust, and sea salt aerosols. The transport, hygroscopic growth of
218 particles, dry and wet removal processes of these particles, and emissions of wind-blown particles
219 are driven by the meteorological fields from the Navy Global Environmental model (NAVGEM,

220 Hogan, et al., 2014). Secondary organic aerosol (SOA) processes are represented with a 1st order
221 approximation method, in which production of SOA from its precursors is assumed to be instant
222 and is pre-treated outside the model. Anthropogenic emissions come from the MACC inventory
223 from ECMWF (Granier et al., 2011). BB smoke emission is derived from the Fire Locating and
224 Modeling of Burning Emissions (FLAMBE, Reid et al., 2009), which is constructed based on the
225 MODIS fire hot spot data. In the reanalysis version, additional orbital corrections and regional
226 emission factors are incorporated. Aeolian dust emissions are determined based on the surface
227 friction velocity to the fourth power, and surface erodibility, which is adopted from Ginoux et al.
228 (2001) with regional tuning. Dust emission occurs when specific conditions related to surface
229 wetness and friction velocity thresholds are met. The representation of sea spray process adheres
230 to Witek et al. (2007), with sea salt emission being governed by sea surface wind conditions.

231 The NAAPS-ReAnalysis (NAAPS-RA) v1 (Lynch et al., 2016) is derived from NAAPS, with
232 assimilation of quality-assured and quality-controlled MODIS (Zhang et al., 2006; Hyer et al.
233 2011) and MISR AOD products (Shi et al., 2011) using 2D-~~variational-var~~ data assimilation
234 method (Zhang et al., 2008). It provides 3-D mass concentration, extinction, and 2-D 550 nm AOD
235 from these aerosol species with 1°x1° latitude/longitude spatial and 6-hourly temporal resolution
236 for the years 2003-2022. The BB smoke source and dust sources are regionally tuned to best match
237 the FM and CM AODs with AERONET AODs. Aerosol wet removals within the tropical region
238 were regulated with satellite precipitation product (Xian et al., 2009) to mitigate model's
239 deficiency to simulate convective precipitation. The reanalysis shows similar decadal trend of
240 AOD found in satellite products (e.g., Zhang et al., 2017) and was verified with various field
241 campaign data (e.g., Reid et al., 2016; Atwood et al., 2017; Edwards et al., 2022; Reid et al., 2023)
242 in addition to ground and space-based observations.

243 2.2 Multi-reanalysis-consensus (MRC)

244 The MRC product is a result of combining four individual aerosol reanalysis products described
245 above. This method follows the multi-model-ensemble approach used by the International
246 Cooperative for Aerosol Prediction (ICAP) and is based on the work by Sessions et al. (2015) and
247 Xian et al. (2019). The data from each RA with spatial resolution different from 1°x1° lat/lon
248 degree, is first projected onto the global map with 1°x1° lat/lon degree resolution using linear
249 interpolation. Then the MRC value is determined by calculating the average of the values from the
250 four RAs. No weighting among the RAs is applied, or the four RAs are weighted equally in
251 deriving MRC. Regionally-weighted ensemble product based on the verification results shown
252 here can be developed in the future. The MRC provides speciated and total AOD at 550 nm with
253 a 1°x1° lat/lon degree -and monthly -resolution for the period ~~2011~~2003-2019. ~~Data~~The MRC data
254 for the period spanning from 2003- to 2010 are available from all-relies on three individual
255 reanalyses exceptRAs, while for the period from 2011 to 2019, it incorporates all four RAs,
256 considering that JRAero- data is only accessible starting from 2011.

257 Table 1. Summary of the characteristics of the aerosol reanalyses.

	Organization	Meteorology	Resolution lat x lon	DA metho	Assimilated obs.	Species	Anthro. & Biogenic Emission	BB Emissions	Available time	reference
CAMSRA	ECMWF	Inline ERA5	0.7 x 0.7	4D-Var	DAQ MODIS PMAp	BC, OM, Sulfate Dust, Sea Salt	MACCcity (trend: ACCMIP + RCP8.5), monthly VOC	GFAS	2003-present	Inness et al., 2019
MERRA-2	NASA	Inline MERRA-2	0.5 x 0.6	2D-Var +LDE	Neural Net MODIS, MISR, AVHRR, AERONET	BC, OC, Sulfate Dust, Sea Salt	EDGAR V4.1, AeroCom Phase II	GFED before 2009, QFED after 2009	1980-present	Randles et al., 2017
NAAPS-RA	NRL	Offline NOGAPS/NAVGEM	1 x 1	2D-Var	DAQ MODIS, MISR	BB smoke, Dust, Sea Salt, ABF	MACCcity, BOND POET, monthly SOA	FLAMBE	2003-present	Lynch et al., 2016
JRAero	JMA	Inline MRI AGCM3	1.1 x 1.1	2D-Var	DAQ MODIS	BC, OC, Sulfate Dust, Sea Salt	MACCcity	GFAS	2011-present	Yumimoto et al., 2017
MRC	-	-	1 x 1	-	-	BB smoke, Dust, Sea Salt, ABF	-	-	2003-present	this work

	Developer	Meteorology	Resolution lat x lon	DA method	Assimilated obs.	Species	Anthro. & Biogenic Emission	BB Emissions	Available time	reference
CAMSRA	ECMWF	Inline ERA5	0.7 x 0.7	4D-Var	DAQ MODIS, AATSR	BC, OM, Sulfate Dust, Sea Salt	MACCcity (trend: ACCMIP +RCP8.5), monthly VOC	GFAS	2003-present	Inness et al., 2019
MERRA-2	NASA	Inline MERRA-2	0.5 x 0.6	2D-Var +LDE	Neural Net MODIS, MISR, AVHRR, AERONET	BC, OC, Sulfate Dust, Sea Salt	EDGAR V4.1, AeroCom Phase II	GFED before 2009, QFED after 2009	1980-present	Randles et al., 2017
NAAPS-RA	NRL	Offline NOGAPS/NAVGEM	1 x 1	2D-Var	DAQ MODIS, MISR	BB smoke, Dust, Sea Salt, ABF	MACCcity, BOND POET, monthly SOA	FLAMBE	2003-present	Lynch et al., 2016
JRAero	JMA	Inline MRI AGCM3	1.1 x 1.1	2D-Var	DAQ MODIS	BC, OC, Sulfate Dust, Sea Salt	MACCcity	GFAS	2011-present	Yumimoto et al., 2017
MRC	-	-	1 x 1	-	-	BB smoke, Dust, Sea Salt, ABF	-	-	2003-present	this work

Table 2. Parameters representing microphysical and optical properties of aerosol species from the four aerosol reanalyses.

Species Models	Microphysics (sectional size bins in radius or bulk effective radius in μm)					Optical parameters at 550nm for the corresponding size bins (single scattering albedo, mass extinction efficiency m^2/g , and shape for dry particle)				
	Dust	Sea salt	sulfate/ABF	BB smoke /OC/OM	BC	Dust	Sea salt	sulfate/ABF	BB smoke /OC/OM	BC
CAMSRA	0.03 - 0.55, 0.55 - 0.9, 0.9 - 20	0.03- 0.5, 0.5 -5, 5 - 20	0.005 - 20	OM: 0.005 - 20	0.005 - 0.5	0.97; 2.56 0.90; 0.92 0.85; 0.42 sphere	1.0; 0.73 1.0; 0.14 1.0; 0.04 sphere	Sulfate 1.0; 4.33 sphere	OM: 0.89; 2.76 sphere	0.21; 9.41 sphere
MERRA-2	0.1 - 1.0, 1.0 - 1.8, 1.8 - 3.0, 3.0 - 6.0, 6.0 - 10	0.03 - 0.1, 0.1 - 0.5, 0.5 - 1.5, 1.5 - 5.0, 5.0 - 10	Bulk, 0.16	OC: Bulk 0.09	Bulk, 0.04	0.96; 2.02 0.92; 0.64 0.89; 0.33 0.83; 0.17 0.77; 0.08 spheroids	1.0; 0.73 1.0; 3.48 1.0; 0.74 1.0; 0.30 1.0; 0.10 sphere	Sulfate 1.0; 3.15 sphere	OC: 0.96; 2.67 sphere	0.21; 9.28 sphere
NAAPS-RAv1	Bulk, 2.5	Bulk, 1.5	Bulk, 0.14	Smoke: Bulk, 0.17	N/A	0.88; 0.59 sphere	0.99; 1.42 sphere	ABF 0.9; 3.48 sphere	Smoke: 0.89; 4.48 sphere	N/A
JRAero	0.100 - 0.159, 0.159 - 0.251, 0.251 - 0.398, 0.398 - 0.63, 0.63 - 1.00, 1.00 - 1.59, 1.59 - 2.51, 2.51 - 3.98, 3.98 - 6.30, 6.30 - 10.0	0.100 - 0.159, 0.159 - 0.251, 0.251 - 0.398, 0.398 - 0.63, 0.63 - 1.00, 1.00 - 1.59, 1.59 - 2.51, 2.51 - 3.98, 3.98 - 6.30, 6.30 - 10.0	Bulk, 0.15	OC: Bulk, 0.18	Bulk, 0.18	0.96; 1.78 0.98; 3.36 0.97; 3.32 0.94; 1.45 0.90; 0.82 0.86; 0.48 0.81; 0.29 0.75; 0.18 0.68; 0.11 0.61; 0.07 sphere	1.0; 0.17 1.0; 0.56 1.0; 1.36 1.0; 1.97 1.0; 1.53 1.0; 0.54 1.0; 0.39 1.0; 0.23 1.0; 0.14 1.0; 0.08 sphere	1.0; 2.26 sphere	0.96; 1.60 sphere	0.16; 5.34 sphere

265 [Table 3. Hygroscopic enhancement factor \(\$f\$ \) at different relative humidity \(RH\) levels for](#)
 266 [various aerosol species in the four RAs. In MERRA-2, \$f\$ for sea salt varies with size bins, thus a](#)
 267 [range for \$f\$ is presented here. Notably, NAAPS-RA v1 does not explicitly contain BC species.](#)
 268 [More specific details can be found in the references provided in Table 1.](#)

RH (%)	Sea salt				Sulfate/ABF				BB smoke/OM/OC				BC		
	CAMSRA	MERRA2	NAAPSRA	JRAero	CAMSRA	MERRA2	NAAPSRA	JRAero	CAMSRA	MERRA2	NAAPSRA	JRAero	CAMSRA	MERRA2	JRAero
<30	1.00	1.00	1.00	1.00	1.00	1.00	1.00	1.00	1.00	1.00	1.00	1.00	1.00	1.00	1.00
30	1.00	1.17-1.22	1.00	1.36	1.00	1.23	1.00	1.24	1.00	1.14	1.00	1.12	1.00	1.00	1.00
40	1.44	1.21-1.28	1.07	1.48	1.17	1.31	1.08	1.32	1.17	1.19	1.03	1.16	1.00	1.00	1.00
50	1.56	1.26-1.35	1.17	1.60	1.22	1.39	1.18	1.40	1.20	1.24	1.06	1.20	1.00	1.00	1.00
60	1.67	1.33-1.44	1.29	1.70	1.28	1.46	1.32	1.45	1.30	1.29	1.11	1.30	1.00	1.01	1.00
70	1.80	1.44-1.56	1.48	1.80	1.36	1.54	1.53	1.50	1.40	1.34	1.16	1.40	1.00	1.03	1.00
80	1.99	1.60-1.77	1.78	2.00	1.49	1.64	1.87	1.60	1.50	1.44	1.25	1.50	1.20	1.19	1.20
85	2.13	1.74-1.93	2.03	2.20	1.58	1.69	2.16	1.70	1.55	1.52	1.32	1.55	1.30	1.30	1.30
90	2.36	1.96-2.19	2.45	2.40	1.73	1.77	2.65	1.80	1.60	1.64	1.42	1.60	1.40	1.41	1.40
95	2.88	2.43-2.74	3.37	2.90	2.09	1.91	3.74	1.90	1.80	1.88	1.61	1.80	1.50	1.54	1.50

270 2.3 AERONET

271 AERONET is a global ground-based sun photometer network managed by NASA. Sun and sky
 272 radiance at multiple wavelengths, covering the near-ultraviolet to near-infrared, are measured
 273 (Holben et al., 1998). Version 3 Level 2 AERONET daily data (Giles et al., 2019), which are
 274 cloud-screened and quality-assured, are used in this study. The estimated uncertainty in
 275 AERONET measured AOD, due primarily to calibration uncertainty, is ~0.01-0.02 at optical
 276 air mass of one for network field instruments (with the highest errors in the UV; Eck et al., 1999).

277 The 550 nm FM and CM AODs and total AODs are derived with the Spectral Deconvolution
 278 Method (SDA; O'Neill et al. 2003). The AERONET SDA product has been verified using in situ
 279 measurements (see for example Kaku et al., 2014). The spectral separation of FM and CM particles
 280 is determined based on their distinctive optical properties and complete size distributions. As part
 281 of this separation, a diameter of approximately 1 μ m serves as an approximate threshold to
 282 differentiate FM and CM particles. This optical separation is different from the sub-micron fraction
 283 (SMF) method that uses a specified cutoff radius of the particle size distribution in the AERONET
 284 (AOD & sky radiance) inversion and allows more data to be available compared to the SMF
 285 method. The FM fraction based on SDA is generally comparable and slightly greater than SMF
 286 (O'Neill et al., 2023).

287 This study uses AERONET sites that have more than 5 years of observations and more than 1000
 288 daily data between 2011 and 2019 for verification purposes. Monthly AOD was derived for months
 289 that have more than 15 days of daily data. Then only sites with more than 45 total number of
 290 months (upper three quartiles of sites regarding total number of monthly data) were selected. This
 291 resulted in a total number of 200 sites globally. ~~A~~The list of [sites along with latitude/longitude](#)
 292 [coordinates and elevation details for the site names studied regions is available accessible](#) in Table
 293 ~~S1 and~~. [Additionally, the locations of these all sites can be found identified](#) in Figure 8.

294 2.4 MODIS AOD

295 ~~MODIS AOD, used for global AOD distribution evaluation of the RAs, was based on Collection~~
296 ~~6.1 Dark Target and Deep Blue retrieval products (Levy et al., 2013). Additional quality~~
297 ~~control. Three MODIS AOD products are used as reference datasets to show global distribution of~~
298 ~~AOD climatology and the divergence among the retrieval products in comparison with the RAs.~~
299 ~~The level 3 MODIS AOD data for Dark Target (DT) were constructed using collection 6.1 Aqua~~
300 ~~MODIS level 2 DT data. The level 2 DT MODIS aerosol retrievals are available at a 10×10 km²~~
301 ~~spatial resolution over both land and ocean. These aerosol retrievals were initially averaged on a~~
302 ~~daily basis at a spatial resolution of 0.5×0.5° lat/lon. Only data with a quality flag of "marginal"~~
303 ~~or better were used in the analysis. Additionally, retrievals with a cloud fraction larger than 80%~~
304 ~~were excluded to minimize cloud contamination, as suggested by Zhang et al. (2005). The level 3~~
305 ~~DT MODIS AOD data (0.5×0.5° lat/lon) were then constructed using the daily averaged AOD~~
306 ~~data.~~

307 ~~Similar approaches were applied to C6.1 Aqua MODIS level 2 Deep Blue (DB) AOD data.~~
308 ~~Unlike the MODIS DT aerosol retrievals, which are available over regions with low surface~~
309 ~~reflectance, the DB retrievals are also available over some bright regions, such as desert regions.~~
310 ~~No over-ocean aerosol retrievals, however, are included in the MODIS level 2 aerosol data. The~~
311 ~~level 2 DB MODIS aerosol data were used to construct daily averages at a spatial resolution of~~
312 ~~0.5×0.5° (lat/lon). No quality flag and cloud fraction thresholds were applied. The level 3 DB~~
313 ~~MODIS AOD data (0.5×0.5° lat/lon) were constructed using the daily averaged AOD data.~~

314 ~~The third MODIS AOD product is a data-assimilation-quality AOD dataset. It was based on C6.1~~
315 ~~DT and DB retrieval products (Levy et al., 2013). Strict quality control and bias-correction~~
316 ~~processes were applied as described in Zhang and Reid (2006) and Shi et al. (2011) for over water,~~
317 ~~Hyer et al. (2011) for over land, and Shi et al. (2013) for over desert regions. These quality control~~
318 ~~processes were updated for the ~~Collection 6C6.1~~ data and the final -MODIS C6.1 AOD (550 nm)~~
319 ~~data is a level 3 product with 1°×1° latitude/longitude/lat/lon spatial and 6-hourly temporal~~
320 ~~resolution. ~~These~~This product has a cut-off at 40°S to filter out potential cloud-contaminated data~~
321 ~~south of this latitude. The 6-hour-averaged MODIS AOD data were then binned into monthly~~
322 ~~means. Note that MODIS AOD products are well known to low bias significant aerosol events~~
323 ~~(Reid et al., 2022; Gumber et al., 2023), which could result in a slightly low AOD climatology,~~
324 ~~especially in source regions.~~

325 ~~Note that MODIS AOD products are well known to low bias significant aerosol events (e.g., Reid~~
326 ~~et al., 2022; Gumber et al., 2023) and slightly high bias clean environment (e.g. Wei et al., 2019),~~
327 ~~which could affect AOD climatology to some degree.~~

328 2.5 Analysis Method

329 This study aims to investigate the ~~diversity~~divergence and utility of RAs for climate-scale studies
330 by exploring the AOD at 550 nm. To achieve this goal, the AOD data from the RAs, as well as
331 MODIS, were spatially and temporally binned into 1°×1° degrees and monthly resolutions. For the
332 purpose of verification and intercomparison analysis, only the data between 2011 and 2019 were
333 used as that is the ~~time~~ period when all the RAs have data. The study focuses on the 550 nm AOD

334 parameter since it is available for all ~~the~~ four aerosol RAs and MODIS. Furthermore, the
335 AERONET FM and CM AODs at 550 nm were obtained using the SDA method described in Sect.
336 2.3.

337 The study examines the performance of RAs globally and regionally. Sixteen regions, including
338 the globe, are defined for regional aerosol property analysis. They include East Asia, Southeast
339 Asia, South Asia, Maritime Continent, Australia, Southwest Asia, Europe, Northwest Africa,
340 South Africa, West North America, East North America, Central America, South America, as
341 indicated by the rectangular boxes in Figure 5, and Arctic (north of 70°N), and Antarctic (south of
342 75°S). There is no AERONET site satisfying site selection criteria as described in Section 2.3 in
343 the Arctic and Antarctic, so these two regions are ~~not included~~excluded for regional verification
344 though they are included in other analyses.

345 Regarding the aerosol species, the study focuses on BB smoke, ABF in NAAPS-RA, and its
346 equivalent of sulfate for MERRA-2, CAMSRA, and JRAero, as well as dust and sea salt. The
347 definition of species follows the ICAP practices (Sessions et al., 2015; Xian et al., 2019) for the
348 operational counterparts of these RAs and previous applications of these RAs (e.g., Xian et al.,
349 2022), in which the sum of ~~Organic Matter (OM)~~ and BC AODs from CAMSRA, and the sum of
350 OC and BC AODs from MERRA-2 and JRAero, is used to approximate BB smoke AODs.
351 Although this separation of species may be somewhat arbitrary, the study takes into account the
352 fact that different aerosol types and sources may be represented differently in each RA. For
353 example, the NAAPS-RA model characterizes aerosol species by emission source rather than
354 chemical speciation, which makes it unique. In contrast, CAMSRA, MERRA-2, and JRAero
355 characterize OM or OC, BC, and inorganic species, merging contributions from various
356 anthropogenic, biomass burning and biogenic sources.

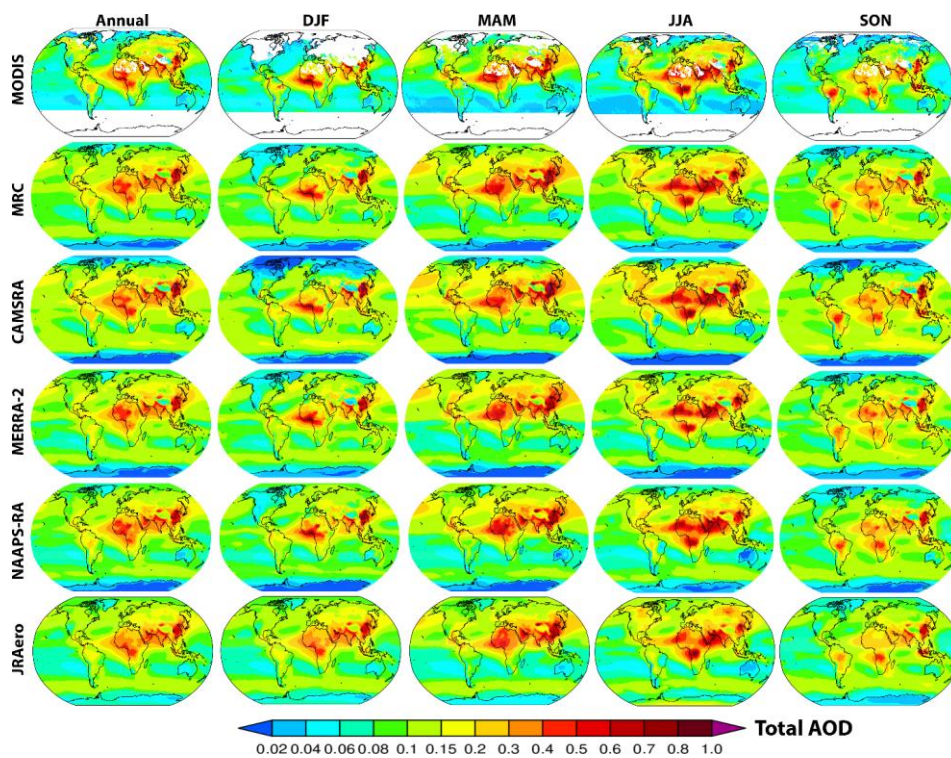
357 The study also assumes that all sea salt and dust are CM, while other aerosol species are FM. The
358 segregation of sea salt and dust to the CM category is based on the fact that only a small portion
359 of ~~total~~ sea salt or dust AOD at 550nm are attributed to their FM components. For example, FM
360 sea salt represents about 17%, 10% and 11% of total sea salt AOD globally in MERRA-2,
361 CAMSRA and JRAero respectively. The numbers are about 30%, 39% and 32% for dust. While
362 FM fraction of dust during dust storms in Africa varies between 20-25% according to AERONET.
363 The FM fraction of dust from MERRA-2, CAMSRA and JRAero might be biased high as these
364 global models tend to overestimate FM dust and underestimate CM dust (for example O'Sullivan
365 et al., 2020; Kramer et al., 2020). In contrast, NAAPS-RA assumes all sea salt and dust are CM.
366 Verification results based on the FM and CM AODs derived using the FM fractions of sea salt and
367 dust from MERRA-2, CAMSRA and JRAero can be found in the supplemental material- (Fig. S2-
368 4). Generally, the validation of FM and CM AODs with AERONET data shows a degradation in
369 performance for the three RAs compared to the verification results presented below, as discussed
370 in section 3.3.1.

371 ~~AOD validation results for total, FM, and CM AOD regarding bias, root mean square error~~
372 ~~(RMSE), and coefficient of determination (r^2) for monthly mean AODs are presented.~~

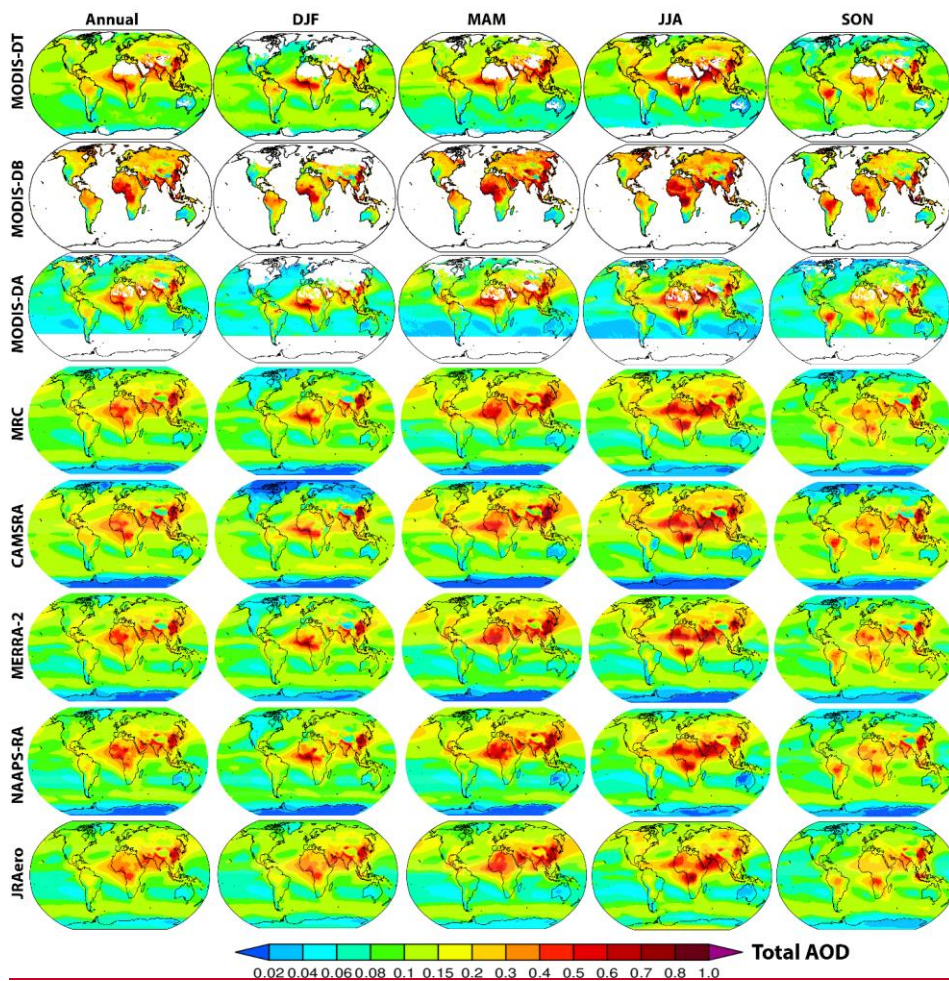
373 For every AERONET site, the time series of monthly modal AOD from each RA is first extracted
374 from the model grid that encompasses the site's location. Bias, root mean square error (RMSE),
375 and coefficient of determination (r^2) are then computed for each site and each RA. The regional
376 validation outcome is derived from the average of validation statistics across all sites within the
377 region (see Table S1 for the sites included in each region). Following the criteria for site selection
378 outlined in section 2.3, only 200 sites are available globally, and certain regions have only a few
379 sites (a minimum of three sites, such as in South Africa) to represent the entire region; hence, no
380 site weighting within a region is applied. It is acknowledged that this averaging method could bias
381 the global validation result toward regions densely populated with sites, notably North America
382 and Europe. The AOD validation results for total, FM, and CM AOD at 550nm are presented
383 accordingly.

384 3. Results

385 3.1 Total and speciated AOD climatology



386

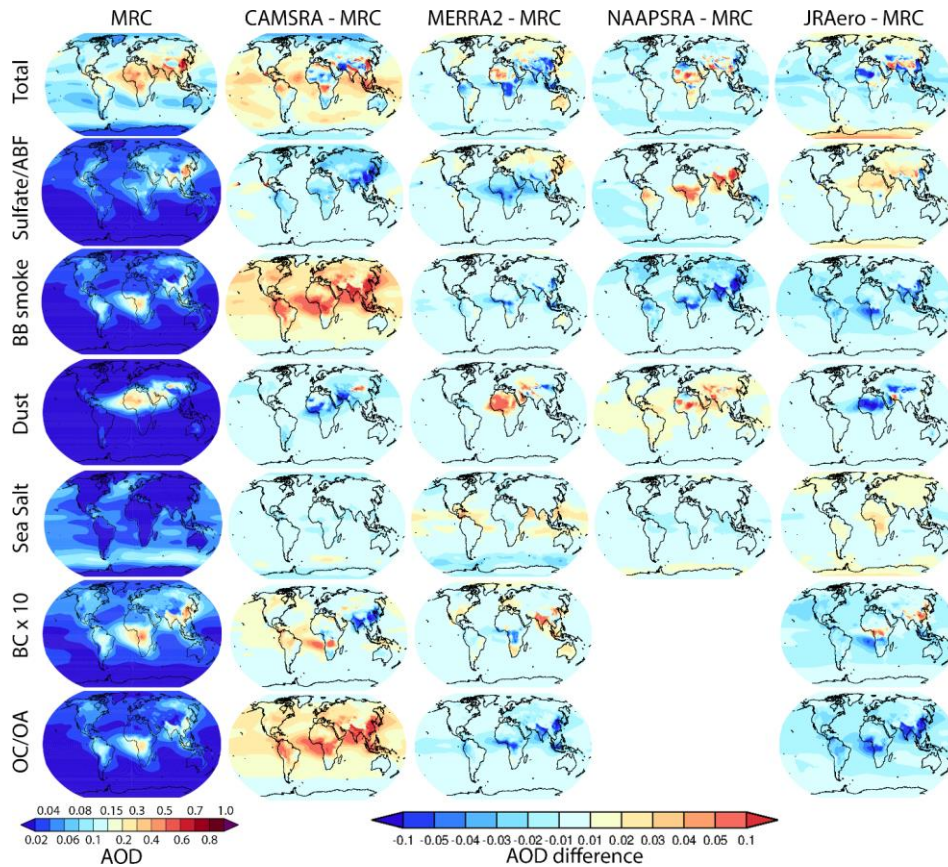


387

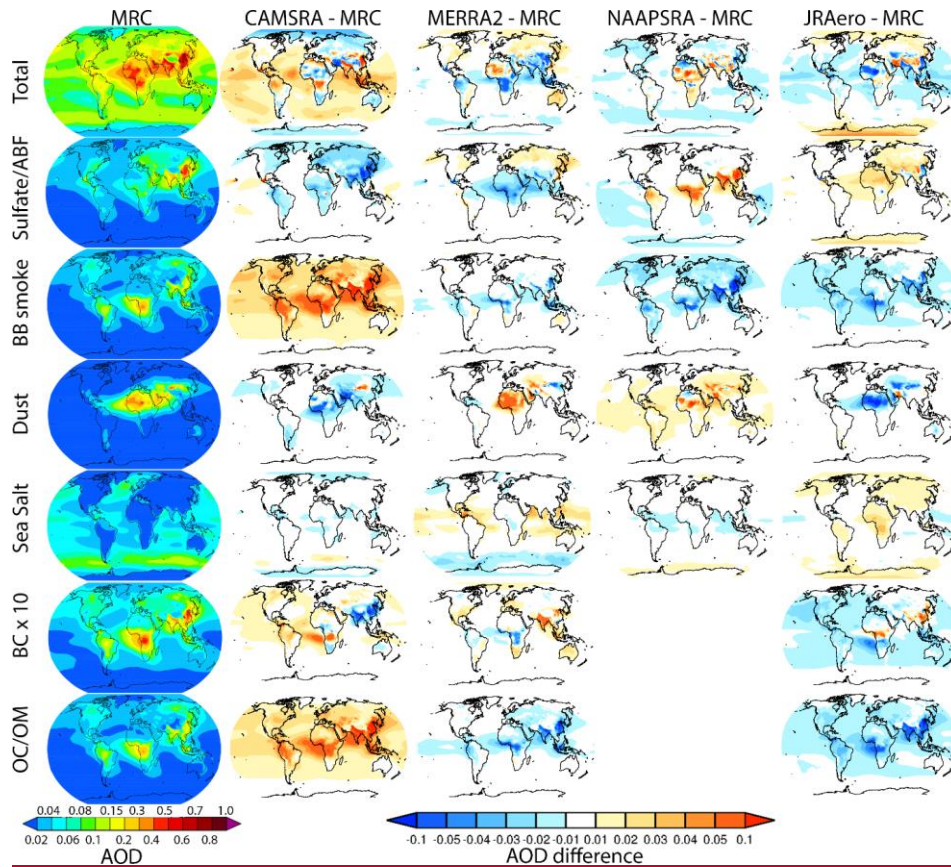
388 Figure 1. Annual and seasonal total 550nm AOD climatology from three MODIS products, the
 389 four RAs, and the MRC over 2003-2019, except JRAero for 2011-2019. The white area-MODIS-
 390 DA is the data-assimilation-quality AOD dataset described in Section 2.4. In the MODIS plots,
 391 the white area means a lack of data- attributed to either none valid-retrievals or quality-control
 392 filtering. Notably, MODIS-DB data is only available over land.

393 The climatological annual and seasonal mean total AODs at 550nm from the three MODIS AOD
 394 datasets and the four aerosol RAs and ~~their consensus~~ (the MRC) are presented in Figure 1. In
 395 general, there are very similar spatial AOD distribution patterns and AOD magnitude among the

396 RAs and MODIS [datasets](#) for all four seasons. This is expected as MODIS total AOD is assimilated
397 into all of these [RA](#) products as well as used to tune the model components such as emissions.
398 High AOD regions include the dust-dominated Sahara in Mar-Apr-May (MAM) and Jun-Jul-Aug
399 (JJA), Sahel in Dec-Jan-Feb (DJF) and MAM, Southwest Asia and Taklamakan in MAM and JJA,
400 anthropogenic pollution-dominated East Asia and South Asia throughout the year, BB smoke-
401 dominated South Africa, South America in JJA and Sep-Oct-Nov (SON), Southeast Asia in MAM,
402 Maritime Continent in SON, and high-latitude North America and Eurasia in JJA. For the annual
403 mean, MODIS ~~AOD is AODs from all the three products are~~ relatively high compared to the MRC
404 in the northern hemisphere's high latitudes due to seasonal sampling bias. MODIS was able to
405 retrieve AOD during biomass burning active season, i.e. boreal Summer-to-Fall, but it couldn't
406 retrieve AOD during northern winter in the high latitudes due to the lack of sunlight, ~~and the high~~
407 ~~snow/ice coverage~~. The high AOD over high-latitude Eurasia and North America in MODIS
408 annual mean is a general reflection of MODIS summertime AOD, which is captured by all the
409 RAs in their summertime mean AODs. ~~It is also noted that all the RAs have slightly higher AOD~~
410 ~~(on the order of 0.02) over the ocean than MODIS QAed product here. MODIS AOD products are~~
411 ~~well known to low bias significant aerosol events (e.g., Reid et al., 2022; Gumber et al., 2023),~~
412 ~~which could lower the mean state of AOD. The slightly lower MODIS AOD compared to the RAs~~
413 ~~could also be related to clear sky and contextual bias (Zhang et al., 2009), as MODIS AOD~~
414 ~~retrieval is only available under clear sky conditions, while all the RAs include all sky conditions.~~
415 ~~Sea salt and dust emissions are often associated with cloudy synoptic weather systems, and~~
416 ~~hygroscopic aerosol species, such as sulfate, sea salt, and BB smoke, can potentially grow larger~~
417 ~~in size in a moister environment, introducing a higher all sky AOD than the clear sky AOD.~~



418
 419 It is worth noting that MODIS-DB AOD generally exhibits slightly higher values compared to
 420 MODIS-DT AOD, except in high terrain regions (e.g., Western North America). On the other
 421 hand, MODIS-DA AOD tends to be slightly lower (approximately 0.02 magnitude) than MODIS-
 422 DT AOD over oceanic regions due to bias-correction procedures. When compared to MODIS-DT,
 423 AODs from the RAs tend to align more closely, especially over oceanic areas. Furthermore, RAs
 424 typically exhibit lower AODs compared to MODIS-DB over regions affected by African and
 425 Arabian dust. Overall, the divergence in total AOD climatology among the RAs is comparable to
 426 or even smaller than the divergence observed in the MODIS products.



427

428 Figure 2. Annual mean total and speciated AODs of the MRC and the AOD difference between
 429 the individual RA and the MRC based on the 2011-2019 average. BB smoke is approximated as
 430 the sum of OC/OM and BC in CAMSRA, MERRA-2 and JRAero.

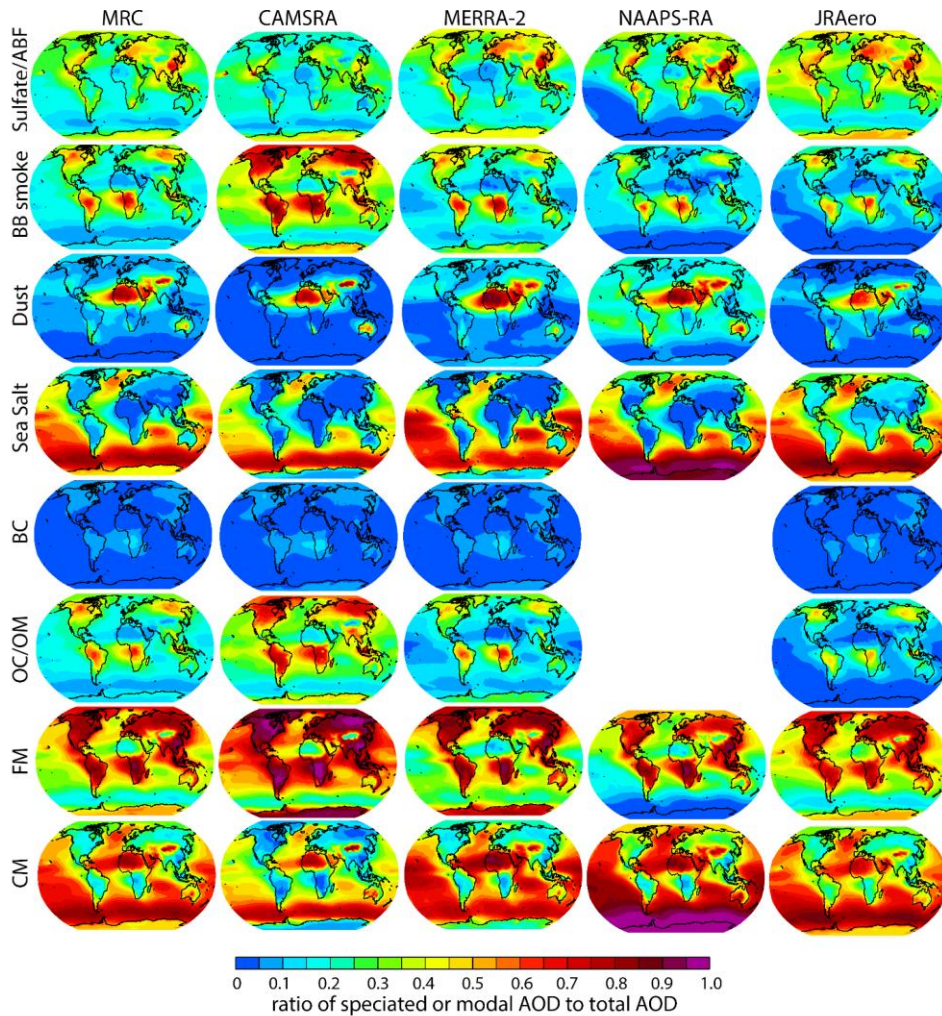
431 Previous experience with multi-model ensembles suggests that the consensus of multi-models, in
 432 general, shows better skill than individual contributing models (Sessions et al., 2015; Xian et al.,
 433 2019; Reid et al., 2022). Similar verification conclusion is also drawn in Section 3.3. Therefore,
 434 the total and speciated AODs from the MRC based on the 2011-2019 average are used as a baseline
 435 here and are shown in Figure 2. As expected, sulfate/ABF AOD is relatively high over population-
 436 dense and industrially polluted regions, dust AOD is high over major desert and arid regions, and
 437 sea salt AOD is relatively high over mid-to-high latitude oceans. BB smoke and its components
 438 BC and OC/OM are relatively high over South Africa, South America, Southeast Asia, the
 439 Maritime continent, and Siberia, North American high latitudes major BB source regions. BC and
 440 OC/OM AOD are also relatively high over South Asia and East Asia, where sources other than

441 BB, such as anthropogenic emission, are the main contributors, as suggested by contrasting smoke
442 AOD contribution to the total AOD between NAAPS-RA and other RAs in these regions
443 (Figures 3 and 10. Noting that smoke AOD is driven by BB in NAAPS-RA, while smoke
444 AOD is a sum of BC and OC/OAOM from the other RAs).

445 Shown also in Figure 2 are the total and speciated AOD differences between the individual RA
446 and the MRC. For total AOD, CAMSRA is apparently higher than the other three RAs over the
447 ocean, which is consistent with the findings on its operational counterpart of high biased FM AOD
448 verified with Maritime Aerosol Network over the ocean in Reid et al. (2022). This high bias is
449 attributed to its universally higher OAOM/smoke AOD compared to other RAs, and suggests that
450 CAMSRA may have higher BB emissions and/or ~~less efficient removal~~ higher secondary
451 production of OM compared to the other RAs. Sulfate AOD is relatively low in CAMSRA except
452 for some highly biased hotspots around outgassing volcanoes (in particular Mauna Loa and near
453 Mexico City) as mentioned in Inness et al (2019). Differences in species definitions affect the
454 comparison with NAAPS-RA: NAAPS-RA ABF AOD is higher than sulfate AOD in other RAs
455 especially in East Asia, South Asia, central Africa, and north South America, and these deviations
456 are counterbalanced by opposite deviations in the BB AOD. This is expected as ABF in NAAPS-
457 RA includes biogenic and anthropogenic primary and secondary aerosols additional aerosol
458 sources besides sulfate, and some of these sources are included in the BB AOD for other models.
459 For dust AOD, MERRA-2 is relatively higher over north Africa and the Arabian Peninsula and
460 NAAPS-RA is relatively higher over most regions, including oceanic areas, while CAMSRA and
461 JRAero are relatively lower over most regions except around Gobi desert for CAMSRA and Iran
462 for JRAero. As for sea salt AOD, MERRA-2 is relatively higher over the tropical oceans, and
463 lower over the southern ocean. JRAero sea salt AOD is relatively higher over most continents,
464 which is probably unphysical.

465 The differences in speciated AOD result in significant variations in their contributions to the total
466 AOD, as illustrated in Figure 3. For instance, the considerably higher BB smoke AOD in
467 CAMSRA compared to other RAs makes BB smoke the predominant contributor to total AOD in
468 the CAMSRA over most continents, adjacent water bodies, and polar regions, except for regions
469 where dust is dominant. Sulfate AOD, on the other hand, contributes more to the total AOD,
470 particularly over oceanic regions in the JRAero compared to other RAs. Both MERRA-2 and
471 JRAero exhibit higher sulfate contributions along the western coasts of South America and North
472 America, suggesting possible increased production of dimethyl sulfide (DMS) in those areas. Dust
473 AOD, on the other hand, contributes more to the total AOD particularly over oceanic regions in
474 NAAPS-RA compared to the other RAs. Sea salt AOD is found to contribute more to the total
475 AOD in the high-latitude oceans and the Antarctic in NAAPS-RA compared to the other RAs. The
476 OC/OAOM AOD contribution to the total AOD closely mirrors the distribution of BB smoke, as
477 anticipated. The contribution of BC to the total AOD is generally small, ranging between 5-10%
478 in BB regions, except for central South Africa where it reaches 10-15%. Despite the higher ratio
479 of BB smoke AOD to total AOD ratio in CAMSRA, the ratio of BC to total AOD over East Asia
480 and South Asia is smaller in CAMSRA compared to MERRA-2 and JRAero, suggesting that BC
481 emissions from anthropogenic sources maybe lower in CAMSRA (also Fig. 2). Finally, the

482 contributions of FM and CM AOD to the total AOD are also depicted in Figure 3. It is consistent
483 among the RAs that FM is the dominant contributor over most land regions except for regions
484 where dust is dominant, such as North Africa, the Arabian Peninsula, the Middle East, and the
485 Gobi. In all the RAs, CM is the dominant contributor over oceanic regions, except for regions
486 influenced by continental BB smoke and pollution outflow. The contribution of CM in CAMSRA
487 is generally smaller in tropical to mid-latitude oceans compared to other RAs, due to its higher
488 contribution from BB smoke. It is also noted that CM is dominant over FM in the Antarctic in
489 NAAPS-RA, while FM is dominant in the Antarctic in the other three RAs, though total AOD is
490 very small (annual and seasonal means < 0.04 from MRC) and hard to validate due to lack of
491 observational data.



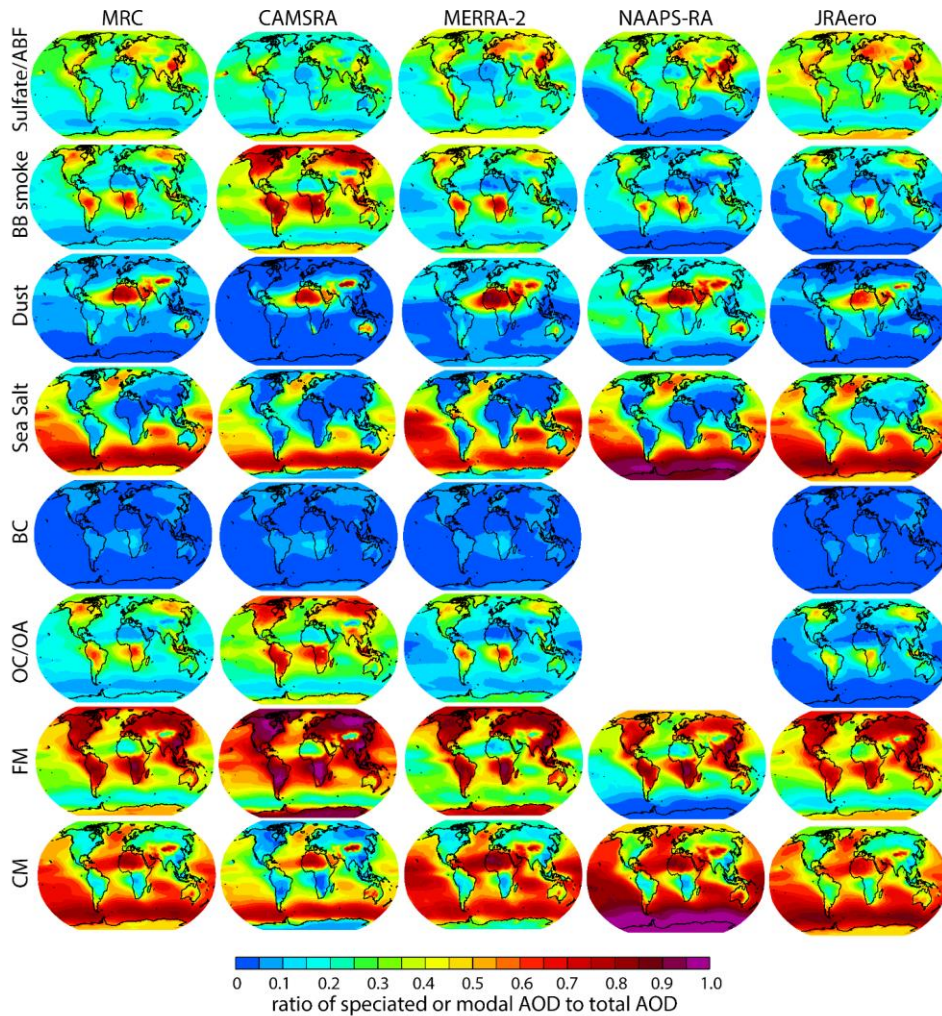
492

493 Figure 3. Ratio of speciated AODs, FM and CM AODs to total AOD from the MRC and the
 494 individual RAs based on the 2011-2019 annual average.

495 Table 24 provides a summary of global-average total AOD and speciated AODs, as well as the
 496 contributions of speciated AOD to total AOD for all the RAs. Overall, the annual and global mean
 497 total AODs are similar, hovering around 0.14 for most RAs. However, CAMSRA stands out with
 498 a slightly higher total AOD of 0.151, which compared to the MRC is 0.012 higher, while the
 499 differences between the other RAs and MRC are within ± 0.005 . Total AODs over land show

500 ~~minimal variation among the RAs, likely due to the cancellation of high and low-biased speciated~~
501 ~~AODs. Over water, CAMSRA exhibits slightly higher AOD compared to other RAs. All land and~~
502 ~~ocean mean AODs are within 0.006 of the MRC with the exception of CAMSRA over ocean,~~
503 ~~which is higher than the MRC by +0.024.~~

504 Speciated AODs, especially smoke AOD and ~~OAOM~~/OC AOD display greater
505 ~~diversity~~divergence among the RAs. Smoke and ~~OAOM~~ AODs from CAMSRA are 2-3 times
506 higher than those from the other RAs. Smoke AOD contributes to 41% of total AOD in CAMSRA,
507 while ranging from 16%-22% in other RAs. Moreover, the standard deviation of smoke and
508 ~~OAOM~~ AODs with respect to the 12 months is also higher in CAMSRA than in other RAs. The
509 contribution of dust AOD to total AOD varies from 13% to 28% for all the RAs, with NAAPS
510 dust AOD being the highest among the RAs and about 2 times that of CAMSRA, which has the
511 lowest dust AOD among the RAs. The contribution of sulfate/ABF AOD to total AOD ranges
512 from 23% to 34%, with the highest contribution observed in JRAero-, even larger than the ABF
513 AOD contribution in NAAPS-RA. Sea salt AOD contributes 25% to 35% to total AOD in the RAs
514 with JRAero being the highest. BC AOD, on the other hand, contributes only 3% to 4% of total
515 AOD across the RAs. The FM's contribution to the overall AOD varies across different datasets.
516 In MERRA-2, NAAPS-RA, and JRAero, FM accounts for 44% to 51% of the total AOD.
517 However, in CAMSRA, its contribution is notably higher at 63%, primarily due to its significant
518 contribution from ~~BBOM~~. Conversely, CM's contribution to total AOD is consistent across the
519 three RAs, ranging from 49% to 56%. In contrast, CM's contribution is lower, at 37%, in
520 CAMSRA.



521

522 **Figure 3.** Ratio of speciated AODs, FM and CM AODs to total AOD from the MRC and the
 523 individual RAs based on the 2011–2019 annual average.

524 Table 24. Global area-weighted mean modal (total, FM, CM) and speciated AOD and standard
 525 deviation of monthly AOD based on 2011–2019 data. Percentage numbers in the brackets are
 526 contributions of speciated AOD to total AOD. Global mean total AODs over land and water are
 527 shown in the last two rows.

Formatted: Font: Times New Roman, 12 pt

	global mean AOD					AOD standard deviation w.r.t. 12 months				
	CAMSRA	MERRA2	NAAPSRA	JRAero	MRC	CAMSRA	MERRA2	NAAPSRA	JRAero	MRC
total	0.151	0.137	0.134	0.134	0.139	0.018	0.010	0.011	0.012	0.013
dust	0.019 (13%)	0.029 (21%)	0.037 (28%)	0.021 (16%)	0.026 (19%)	0.008	0.009	0.009	0.009	0.008
sea salt	0.037 (25%)	0.041 (30%)	0.038 (28%)	0.045 (34%)	0.040 (29%)	0.001	0.001	0.003	0.002	0.001
sulfate/ABF	0.034 (23%)	0.037 (27%)	0.037 (28%)	0.046 (34%)	0.039 (28%)	0.002	0.001	0.001	0.002	0.001
smoke	0.062 (41%)	0.030 (22%)	0.022 (16%)	0.022 (16%)	0.034 (24%)	0.009	0.007	0.007	0.007	0.007
BC x 10	0.061 (4%)	0.059 (4%)		- 0.044 (3%)	0.054 (4%)	0.013	0.009	-	0.008	0.009
OC/OA	0.056 (37%)	0.024 (18%)		- 0.018 (13%)	0.033 (24%)	0.007	0.006	-	0.006	0.006
FM	0.096 (63%)	0.067 (49%)	0.059 (44%)	0.068 (51%)	0.073 (53%)					
CM	0.056 (37%)	0.070 (51%)	0.075 (56%)	0.066 (49%)	0.066 (47%)					
land total	0.180	0.174	0.175	0.176	0.176					
water total	0.136	0.118	0.112	0.111	0.112					

528

	global mean AOD					AOD standard deviation w.r.t. 12 months				
	CAMSRA	MERRA2	NAAPSRA	JRAero	MRC	CAMSRA	MERRA2	NAAPSRA	JRAero	MRC
total	0.151	0.137	0.134	0.134	0.139	0.018	0.010	0.011	0.012	0.013
dust	0.019 (13%)	0.029 (21%)	0.037 (28%)	0.021 (16%)	0.026 (19%)	0.008	0.009	0.009	0.009	0.008
sea salt	0.037 (25%)	0.041 (30%)	0.038 (28%)	0.045 (34%)	0.040 (29%)	0.001	0.001	0.003	0.002	0.001
sulfate/ABF	0.034 (23%)	0.037 (27%)	0.037 (28%)	0.046 (34%)	0.039 (28%)	0.002	0.001	0.001	0.002	0.001
smoke	0.062 (41%)	0.030 (22%)	0.022 (16%)	0.022 (16%)	0.034 (24%)	0.009	0.007	0.007	0.007	0.007
BC x 10	0.061 (4%)	0.059 (4%)		- 0.044 (3%)	0.054 (4%)	0.013	0.009	-	0.008	0.009
OC/OM	0.056 (37%)	0.024 (18%)		- 0.018 (13%)	0.033 (24%)	0.007	0.006	-	0.006	0.006
FM	0.096 (63%)	0.067 (49%)	0.059 (44%)	0.068 (51%)	0.073 (53%)					
CM	0.056 (37%)	0.070 (51%)	0.075 (56%)	0.066 (49%)	0.066 (47%)					
land total	0.180	0.174	0.175	0.176	0.176					
water total	0.136	0.118	0.112	0.111	0.112					

529

530 3.2 Geographical diversitydivergence of speciated AOD among the four reanalysesRAs

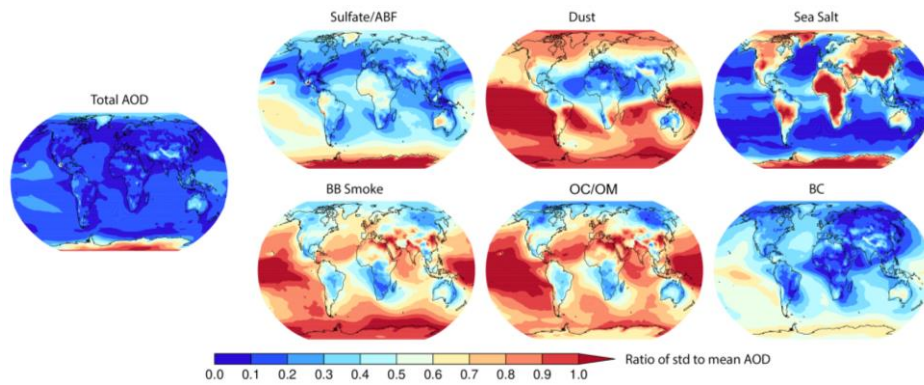
531 The diversitydivergence of the global-average total and speciated AODs is already documented in
532 Table 24. Figure 4 provides the geographical distribution of the relative spread of speciated annual
533 mean AODs from the RAs to their means. Spread, in this context, is defined as the ratio of the
534 standard deviation of the RAs AODs to their mean. It is noteworthy that the relative spread of total
535 AOD from the four RAs is generally small, except for polar regions and specific hotspots where
536 known issues exist. For instance, biases in CAMSRA AOD have been identified over Hawaii and
537 Mexico's volcanic outgassing regions. In polar regions, there are limited satellite observations to
538 constrain model fields, resulting in a larger spread, which is consistent with the findings of Xian
539 et al. (2022) on AODs from CAMSRA, MERRA-2 and NAAPS-RA over the Arctic. Similarly,
540 over high terrains with snow and ice covers, such as the Himalayas and the Andes, and over desert
541 regions, such as the Australian deserts, and the Bodele Depression region in the Sahara, both
542 retrievals and models face challenges, leading to a larger spread. Moreover, over the Maritime
543 Continent, where high cloud coverage poses challenges to remote sensing retrievals for both AOD
544 and BB smoke emissions, the spread is also relatively large.

545 The aforementioned characteristics are also evident in the spread of speciated AODs. However,
546 the spreads of the speciated AODs among the RAs are much larger compared to the total AOD,
547 particularly in regions that are remote from aerosol sources. This suggests that the efficiency of
548 removal processes during long-range transport may differ. This is also relevant to the fact that data

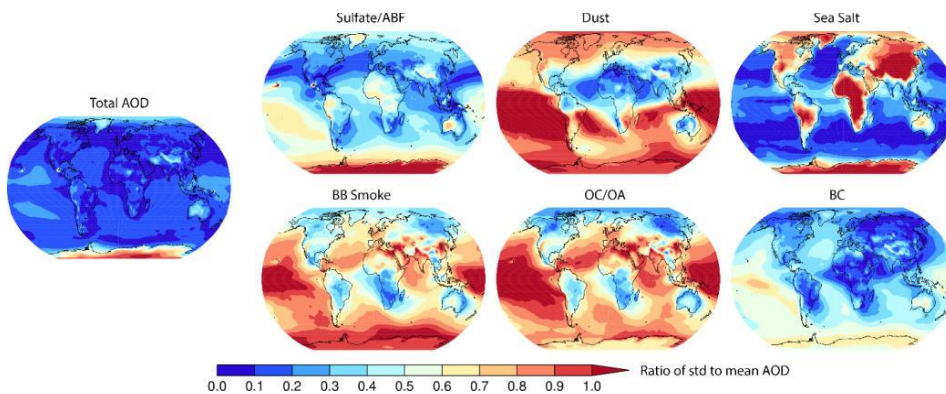
549 assimilation constrains the total AOD, but speciated AOD remains unconstrained. Moreover, the
 550 disparities in definitions of species, such as sulfate/ABF, BB smoke, OC/OAOM, as discussed in
 551 Section 2.5, can also influence the spread of these FM species. The relative spread of speciated
 552 AODs being much larger than that of total AOD, is broadly consistent with the AeroCom results,
 553 where global climate models (without data assimilation) were intercompared in terms of aerosol
 554 optical properties and life cycles (Kinne et al., 2006; Textor et al., 2006; Gliß et al., 2021).

Formatted: Font color: Black

555



556



557

558 Figure 4. Spread of total and speciated climatological annual-mean AOD among the four RAs.
 559 Spread here is defined as the ratio of the standard deviation of the RA AODs to their mean.

560 **3.3. Evaluation with AERONET AOD**

561 This section presents evaluation of the monthly performance of the four RAs plus the
 562 consensusMRC at the AERONET sites on regional and global scales. Both skill and consistency
 563 of the different RAs and consensus are evaluated.

564 **3.3.1 Bias, RMSE, and correlation between the RAs and AERONET**

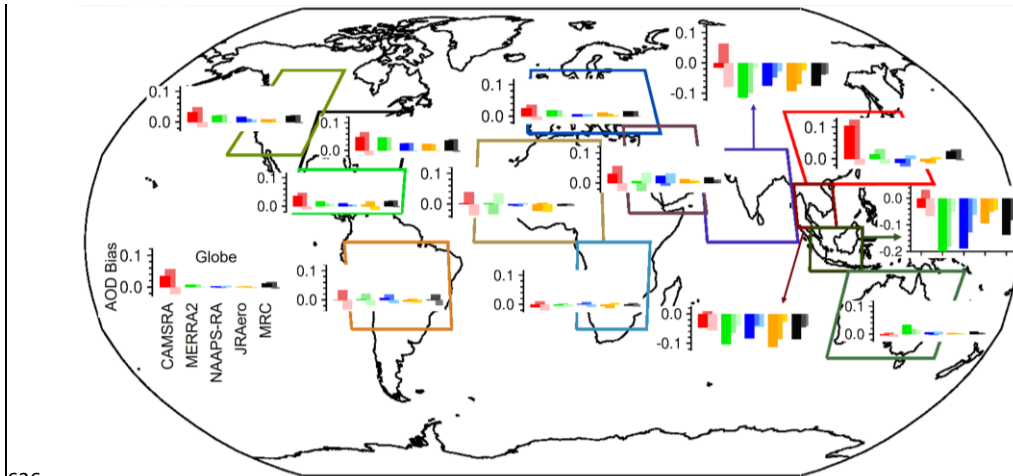
565 The regional and global mean modal AOD bias, RMSE, and ~~square coefficient~~ of ~~the~~
566 ~~correlations determination~~ for the four RAs and the MRC are shown as bar graphs on global maps
567 in Figures 5, 6 and 7. Regarding regional bias, all the RAs except for CAMSRA, have large
568 negative biases (on the order of -0.1) in total AOD over Southeast Asia, South Asia, and the
569 Maritime continent (Figure 5). The much smaller negative bias in total AOD over these regions in
570 CAMSRA is a result of the cancelation of a positive bias in FM, possibly due to high biased
571 ~~QAOM~~/smoke AOD, and a negative bias in CM. The large negative biases over these regions in
572 the other RAs are mainly attributed to large negative biases in FM AOD in general. It is also noted
573 that CAMSRA is biased relatively high in total AOD due to high FM bias over East Asia. Over
574 other regions and the globe, all the RAs have relatively small biases and in general slight positive
575 biases, with CAMSRA having the largest positive bias, due mainly to relatively high
576 ~~QAOM~~/smoke AOD. The cancellation effect of positive FM bias and negative CM bias in
577 CAMSRA are also visible.

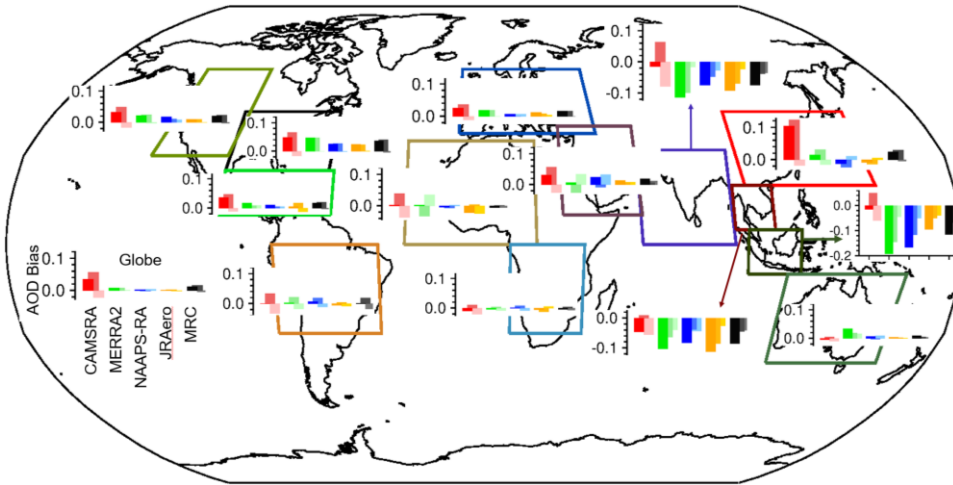
578
579 Total AOD RMSEs are relatively high over all Asian regions and North Africa compared to other
580 regions for all the RAs (Figure 6). The contribution of FM to total AOD RMSE is larger than that
581 from CM globally, except over dust-influenced ~~regions region~~, including North Africa and, for
582 most models, Southwest Asia and Central America. The correlations of total AOD between the
583 RAs and AERONET data are mostly reasonable for all the regions (Figure 7). Some relatively
584 low-performance regions (total AOD r^2 less than 0.60 for at least one RA) include South Asia,
585 Southwest Asia, Australia, Europe, and East Asia. The relatively low correlations over Australia
586 and Europe are due to the low climatological mean and variance. While the other low-performance
587 regions are all mixed pollution and dust environment that is challenging for all RAs. Some
588 relatively high-performance regions (total AOD r^2 greater than ~~0.9085~~) for at least two RA
589 members) include Central America, Peninsula Southeast Asia, and Maritime Continent. Total and
590 CM AOD r^2 are high over Central America, because it is a receptor region for African dust, and
591 RAs perform well in general during long-range transport over ocean where data assimilation is
592 very effective in correcting model AOD fields. Total and FM AOD r^2 are high over Peninsula
593 Southeast Asia, and Maritime Continent, ~~because suggesting the RAs can capture the large~~
594 ~~interannual variabilities of~~ the regional dominant aerosol species, BB smoke, ~~have large~~
595 ~~interannual variabilities, due to associated with~~ the impact of ENSO on fire activities in the regions
596 (e.g., Reid et al., 2012; Xian, et al., 2013). Overall, the MRC exhibits superior r^2 compared to
597 individual RAs for modal AODs regionally and globally.

598
599 For remote marine sites, including Ascension Island in the mid-basin of south Atlantic, Ragged
600 Point in the western Tropical Atlantic, Mauna Loa in Hawaii, MCO-Hanimaadhoo in the north
601 Indian Ocean, and REUNION_DENIS in the south Indian Ocean, the RAs exhibit similar
602 performance at these sites as they do over the upwind land or coastal regions (Fig. S1). An
603 exception is ~~Mauna~~Mauna Loa. ~~Mauna~~Mauna Loa is situated at an elevation of 3.4 km, well above
604 the marine boundary layer and remote from continental sources. At this location, all the RAs
605 exhibit a significant positive bias. One possible explanation for this bias is the topographic effect,
606 as the coarse spatial resolutions of the models may not be able to resolve the site's high elevation-
607 ~~or its sharp elevation gradient compared to the surroundings~~. Additionally, uncertainties in the
608 removal processes during long-range transport may also be contributing to the high bias. ~~It is also~~
609 ~~worth noting that all the RAs do especially well at the Ragged Point site, with total AOD r^2 close~~

611 [to or higher than 0.92. This site is a receptor site of African dust in the Western Tropical Atlantic.](#)
612 [This suggests that the RAs capture the long range-transport of dust from Africa quite well. This is](#)
613 [related to the fact that data assimilation systems have more chance to correct the model fields with](#)
614 [observations in the long-range transport over the ocean.](#)

615
616 When considering the contribution of dust and sea salt aerosols to FM AOD in CAMSRA,
617 MERRA-2 and JRAero, the verification statistics (bias, RMSE and r^2) for the total AOD of these
618 RAs remain unchanged as expected (Fig. S2, S3, S4). However, there is a noticeable shift in the
619 positive bias of FM AOD (and negative bias of CM AOD) for these RAs, particularly in regions
620 influenced by dust, such as North Africa, the Arabian Peninsula, East Asia, Central America, South
621 Asia, and Europe. Specifically, the positive bias in FM AOD becomes more pronounced, and the
622 negative bias in CM AOD becomes more negative in these regions, especially for CAMSRA. It's
623 worth noting that in MERRA-2, there is a change in sign, where the FM AOD bias switches from
624 negative to positive in North Africa and the Arabian Peninsula, while the CM AOD bias changes
625 from positive to negative in these regions. Additionally, the negative FM AOD bias becomes
626 smaller, however the negative CM AOD bias worsens in South Asia within both MERRA-2 and
627 JRAero datasets (Fig. S2). In general, when taking into account the contribution of dust and sea
628 salt aerosols to FM AOD (by default, dust and sea salt AODs are treated as CM AODs in this
629 study) in CAMSRA, MERRA-2, and JRAero, we observe a worsening of both FM and CM AOD
630 biases in these three datasets. Similarly, the RMSE for both FM and CM AODs over regions
631 influenced by dust deteriorates as well (Fig. S3). The r^2 for FM and CM AODs in these regions
632 also worsens overall, with the exception of an improvement in FM AOD over Central America.
633 FM sea salt's impact on the verification score is small as the majority of AERONET sites are on
634 land and FM sea salt only contributes on the order of ~10% to total sea salt AOD in the three RAs.
635

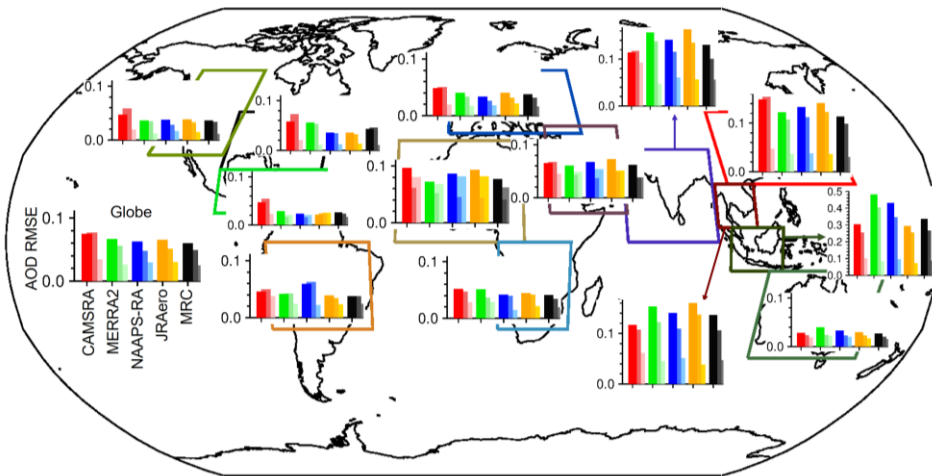




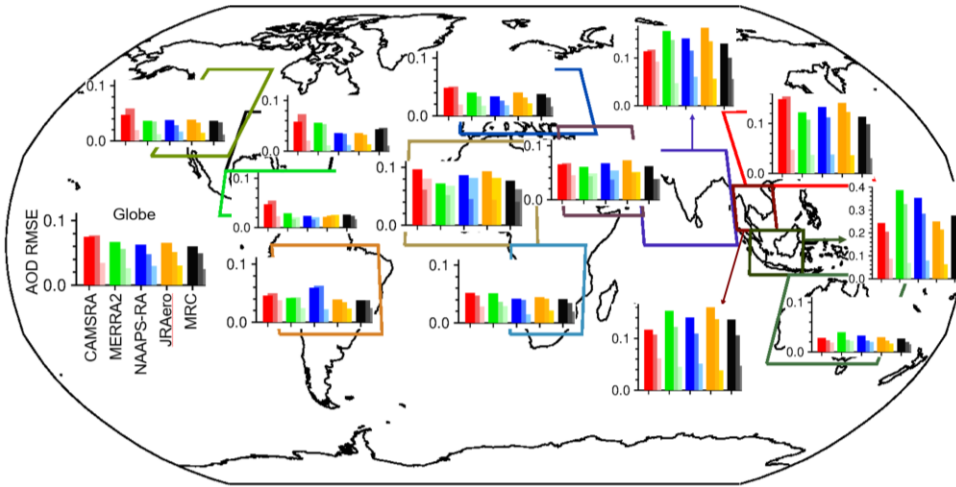
637

638 Figure 5. Regional total, FM, and CM AOD biases for the four reanalyses and the MRC
 639 compared with AERONET data. Each grouped bars in the same color system present total, FM,
 640 and CM AOD biases from left to right (also dark to light).
 641

642

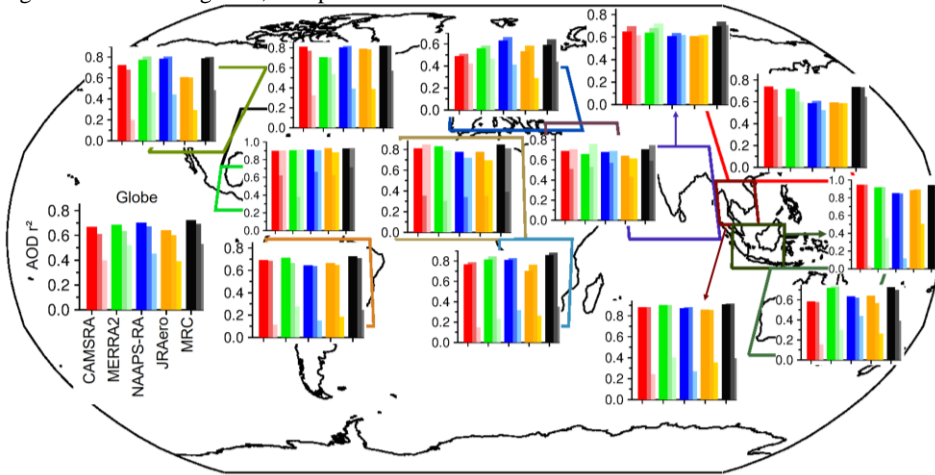


643

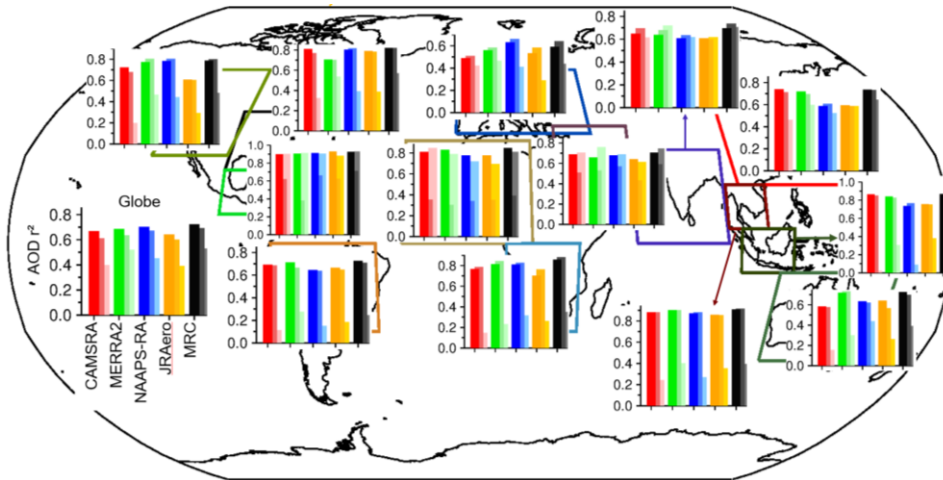


644
645
646

Figure 6. Same as Figure 5, except for AOD RMSE.



647



648

649 Figure 7. Same as Figure 5, except for the AOD coefficient of determination (r^2).

650

651

652

3.3.2 Rankings of the RAs with respect to validation statistics

653

654

655

656

657

658

659

660

661

662

663

664

To expand the validation result from regional averages to individual sites, including remote sites that are not included in the regional analysis, rankings of the RAs in terms of RMSE of monthly total AOD at all the AERONET sites are displayed in Figure 8. It shows that there are cases in that individual RA ranks first over some regions. For example, CAMSRA ranks relatively better than others in South and Southeast Asia, MERRA2 ranks better over North Africa and Arabia Peninsula, NAAPS-RA ranks better over North America and Europe while JRAero performs relatively better over Southern North America and the Caribbean. Individual reanalysisRA has mixed results for sites in other regions. AOD RMSE of the MRC is not always the lowest for a given site, but it is relatively low and stable over the globe. This is consistent with the regional RMSE result (Figure 6). The consensus wins because of its averaging of independent models. This is consistent with our findings with the ICAP models- ([Sessions et al., 2015](#); [Xian et al., 2019](#)).

665

666

667

668

669

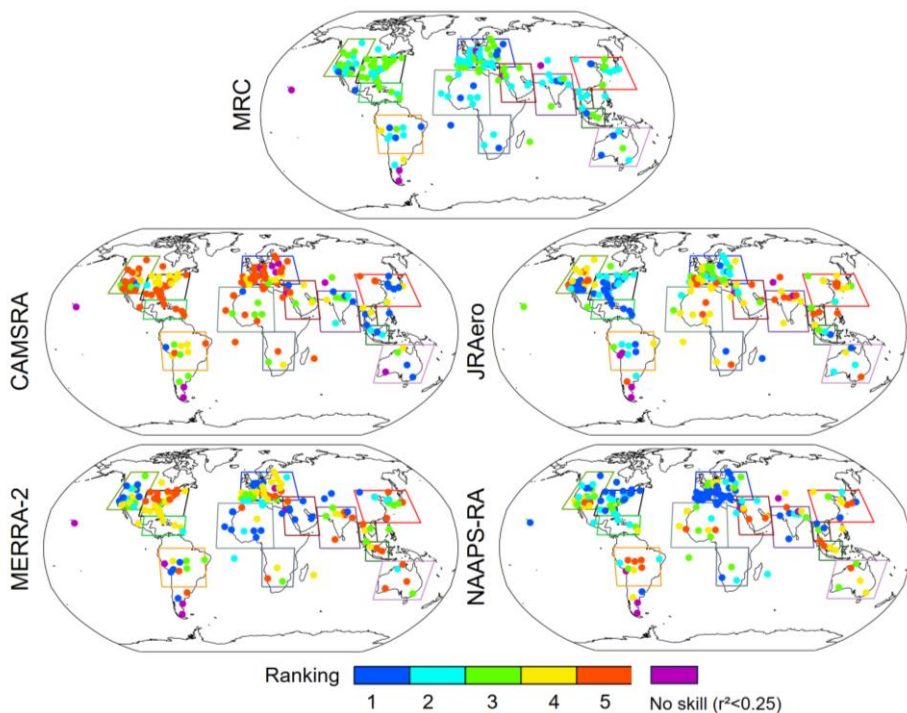
670

671

672

673

Challenging sites for these RAs are found as marked by the magenta color in Figure 8. These sites exhibit an r^2 value of less than 0.25, and are associated with relatively large AOD bias and/or RMSE. Often, when a challenge occurs, it is a common challenge to all models, and no specific model is much better than the others. Some of the causes for the challenges include lack or large uncertainty in local emissions (e.g. Modena in Northern Italy, Mainz in Germany, Cario_EMA in Egypt, Trelew and CEILAP-RG sites in Argentina), and/or topographic effects that are not resolved in these RAs due mostly to coarse model spatial resolutions (e.g., Mauna_Loa), and sites that are impacted by mixed pollution and dust (Dushanbe in Tajikistan).



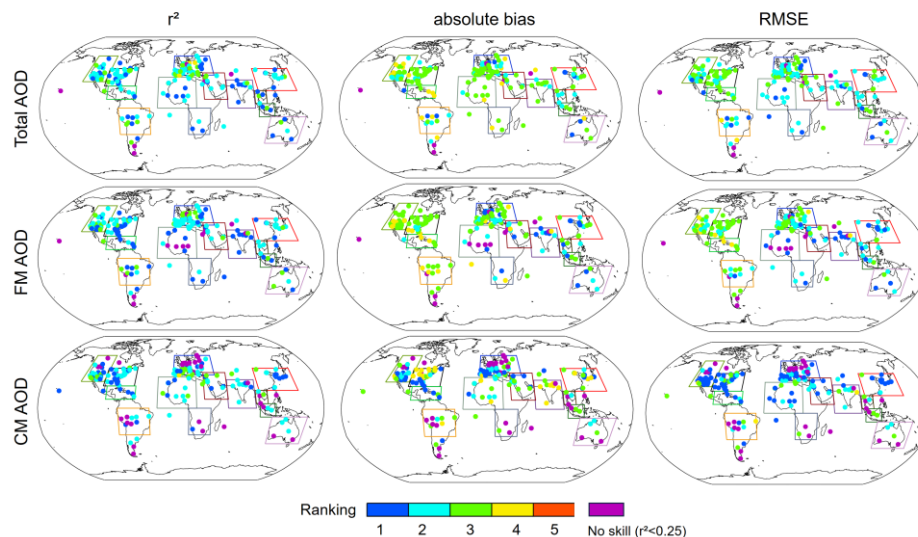
674

675 Figure 8: Ranking of aerosol RAs in terms of RMSE of monthly total AOD at 550nm over all the
 676 AERONET sites. Rectangles are used to delineate regions for regional validation, as depicted in
 677 Figures 5, 6, 7. A lower RMSE indicates better performance, with a ranking of 1 being the most
 678 desirable. AERONET sites with a coefficient of determination (r^2) less than 0.25 are marked in
 679 magenta, indicating a lack of skill from the model.

680

681 Ranking analyses were also conducted on the RMSEs of FM and CM AODs, absolute bias, and
 682 **coefficient of determination (r^2)** of modal AODs. Figure 9 presents the MRC rankings for all these
 683 comparison statistics. In line with the MRC ranking for the total AOD's RMSE, the MRC rankings
 684 for other metrics are predominantly ranked first or second, except for the absolute biases, where
 685 MRC rankings are often ranked third over North America, South Americas, and Europe for total
 686 and FM AODs. For these modes and over these regions, all the RAs have positive biases relative
 687 to AERONET. When the biases are in the same sign (positive or negative), it is mathematically
 688 natural for MRC to rank in the middle. For CM and FM AODs, there are more sites with $r^2 < 0.25$
 689 compared to the total AOD. These sites mostly have small values of CM or FM AODs, and reside
 690 in regions of opposite-mode dominance, such as FM in Saharan region, CM in northern Europe
 691 and N. America. From another perspective, the MRC ranking with respect to correlations is
 692 superior to RMSE and then absolute bias. That is, the MRC better captures aerosol variance than
 693 the individual models, but is nevertheless subject to overall model biases. The MRC ranking for
 694 CM AOD is slightly superior to that of total AOD and then FM AOD. While the MRC ranking is

695 not consistently at the top for a given site or region, it is relatively high and stable, ranking first
 696 for the global average. No individual RAs could compete with the MRC in that sense.



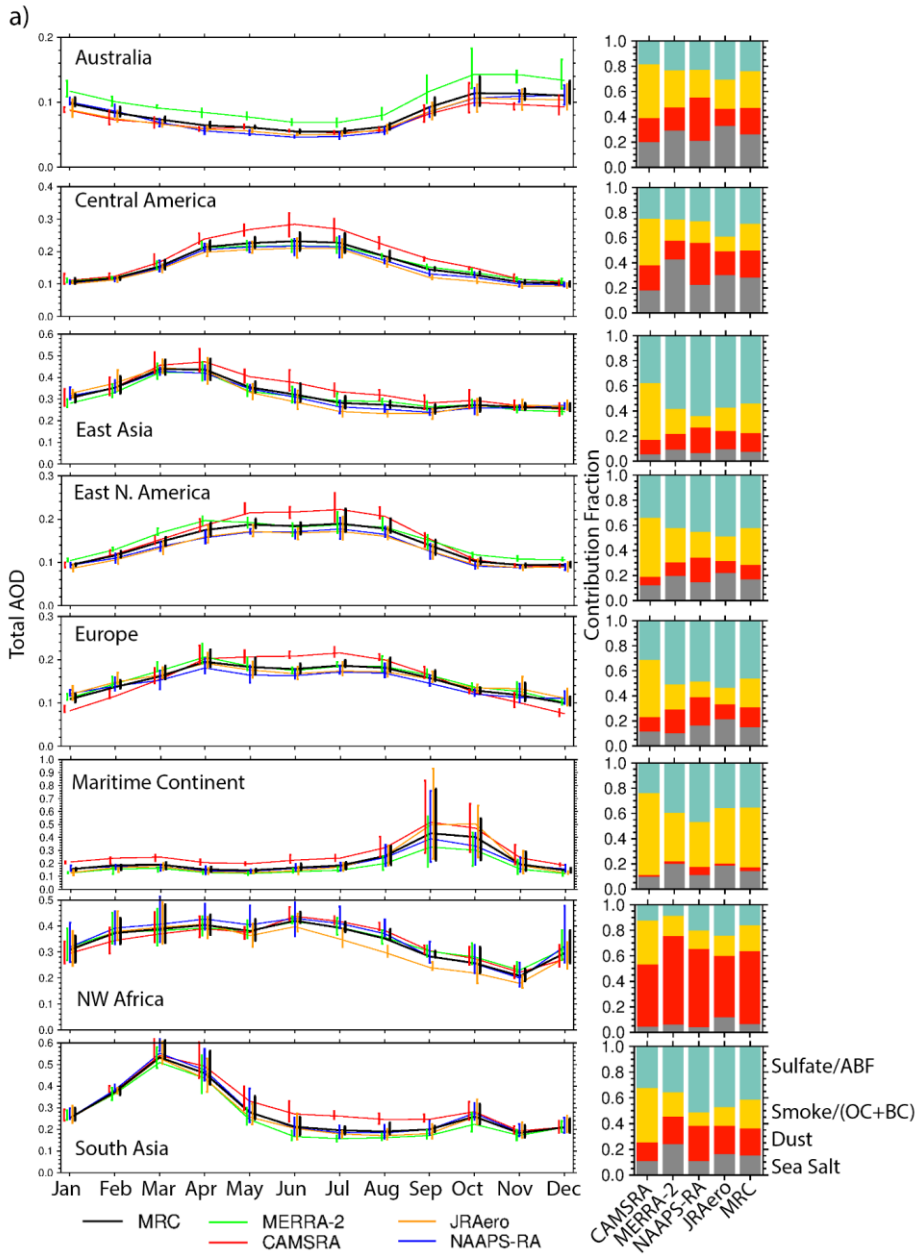
697 Figure 9. Ranking of the MRC among all the RAs in terms of r^2 , absolute bias, and RMSE of the
 698 total, FM, and CM AODs over AERONET sites.
 699

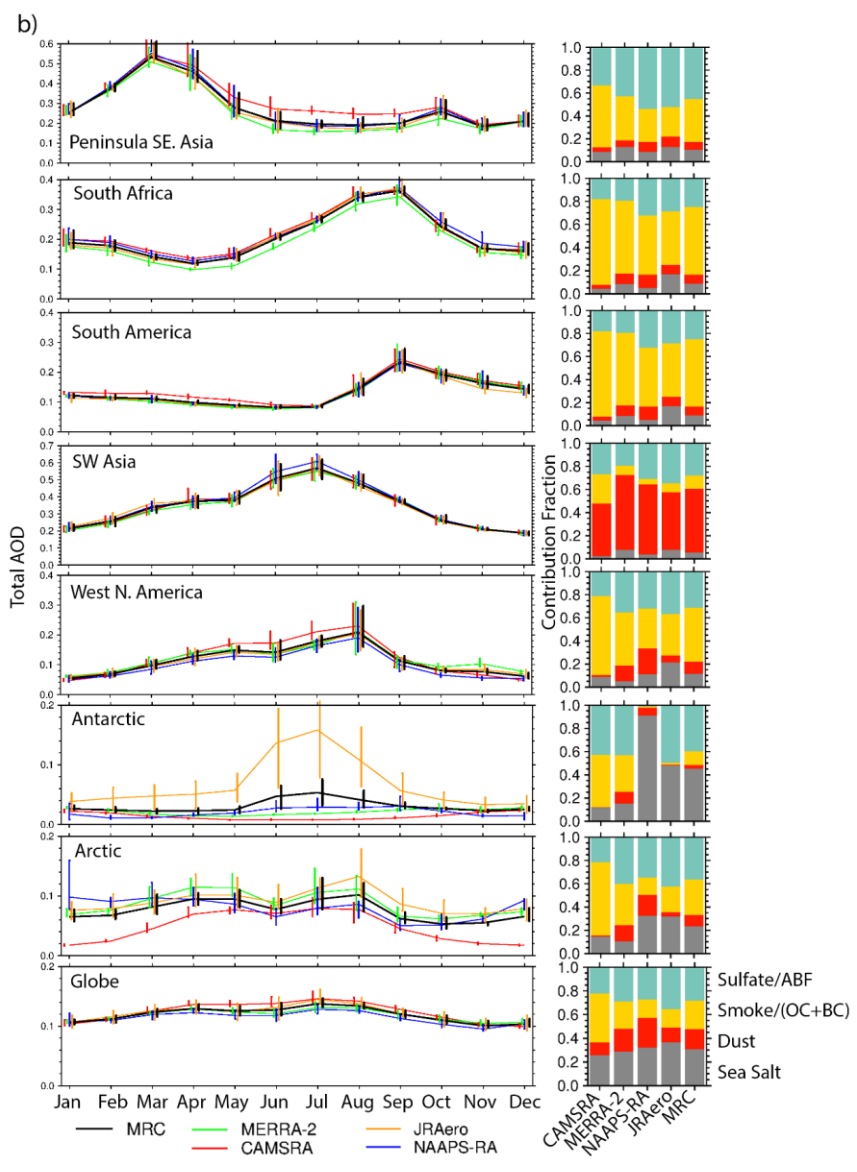
700 3.4 Seasonality of Regional AODs

701 In Section 3.1 we depict the spatial distribution of total AODs from all the RAs across the four
 702 seasons. In this section, we provide monthly time series of AOD and AOD interannual variabilities
 703 for 16 regions (Fig. 10), along with the contributions of speciated AOD to the total AOD for these
 704 regions- for four seasons and the annual-mean. All the RAs exhibit a similar seasonality and
 705 interannual variability of total AOD for all regions, except for the Antarctic and Arctic, particularly
 706 during their winter seasons. This disparity arises from the absence of passive satellite AOD data
 707 during polar winter, which limits the effect of data assimilation on model AOD (see Xian et al.,
 708 2022 for the Arctic region). Even during polar summer, AOD retrievals are often unavailable due
 709 to high reflectance from surface ice/snow. ~~The polar regions demonstrate the most significant
 710 diversity among the RAs in the seasonal cycle and speciation of AOD.~~ The total AOD in JRAero
 711 exhibits exceptionally high levels, primarily attributed to elevated sea salt and sulfate AODs (Fig.
 712 S5). This anomaly stems from the MASINGAR model used to produce JRAero, which tended to
 713 underestimate the removal of aerosols via cumulus convection. Consequently, this led to an
 714 overestimation of aerosol concentrations in the polar regions and the upper atmosphere. The
 715 underestimation of the removal process has been resolved in the current MASINGAR model and
 716 the overestimation of AOD over the polar regions will be improved with the JRAero version
 717 upgrade. Nevertheless, the polar regions demonstrate the most significant divergence among the
 718 RAs in the seasonal cycle and speciation of AOD.
 719

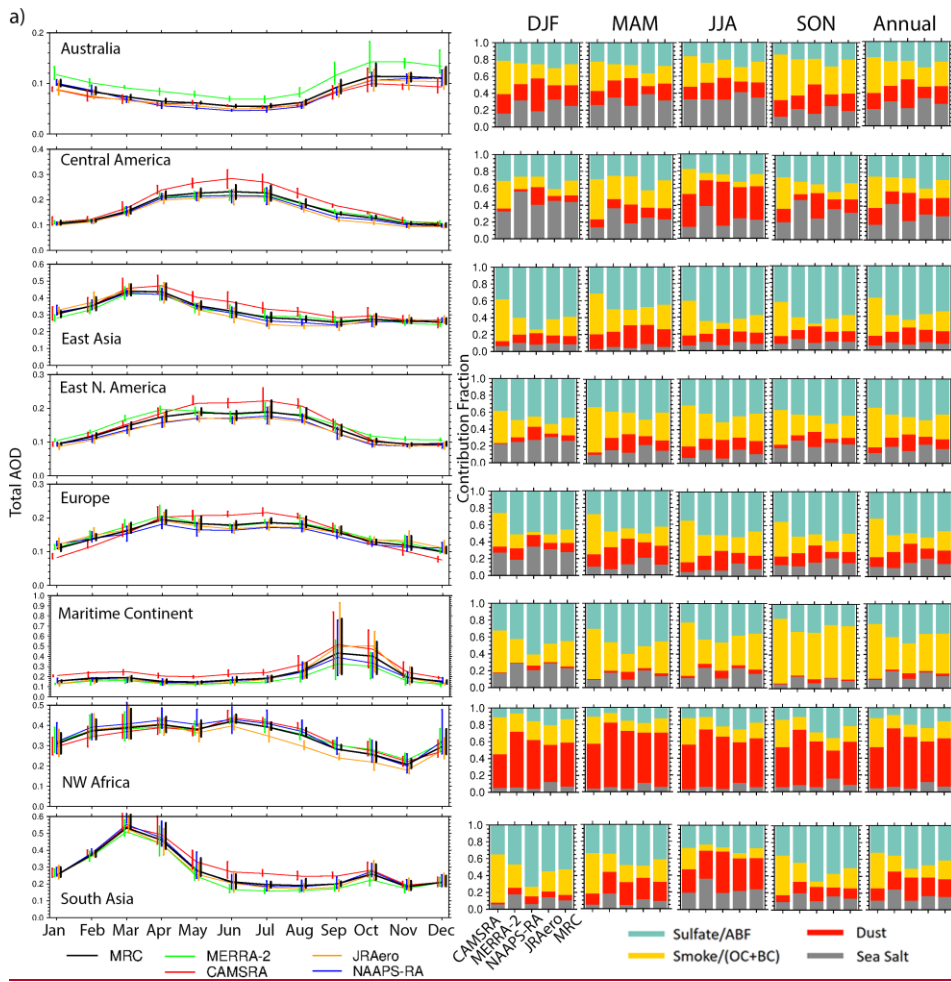
720 The regions that are dominated by BB-smoke, including South Africa, South America, Maritime
 721 Continent, Peninsula SE Asia, and western North America, exhibit consistent peak seasons of total
 722

723 AOD with their respective burning seasons. The Maritime Continent and Peninsula SE Asia
724 experience extremely large interannual variations of peak monthly AOD, owing to a strong
725 positive correlation between burning activities and El Nino cycles (e.g., Reid et al., 2012; Xian et
726 al., 2013). The contributions of sulfate/ABF AOD induced by pollution are dominant in East Asia
727 and South Asia, while other aerosol species also make a significant contribution to the total AOD.
728 In Europe and East N. America, sulfate/ABF is also the dominant species; however, the monthly
729 total AOD values are much smaller. All the RAs capture the dominance of dust species in
730 summertime over SW Asia and NW Africa. The relatively high AOD in springtime in NW Africa
731 is partially due to BB in Sahel. In Australia, the peak AOD in Oct-Dec is associated with BB
732 smoke. In Central America, the relatively high AOD in the springtime results from BB smoke.
733 Although quite diverse in AOD magnitude, all RAs tend to have a summertime total AOD peak
734 attributed to dust. For the global average, sea salt AOD has a significant contribution to the total
735 AOD as the area of the ocean overwhelms the area of land. Monthly time series of the speciated
736 AODs for all the regions are available in ~~the Figure~~Fig. S5. Overall, the seasonality and interannual
737 variability of total AOD for most regions is very similar among the RAs. Moreover, all RAs have
738 the same dominant species for most regions, but the contributions from different species can be
739 quite different in these RAs. This is a result of the fact that total AOD is constrained within these
740 RAs through data assimilation, while speciated AODs are not. Aerosol speciation and the
741 contribution of each species to the total AOD are determined by the construction of the aerosol
742 forecast models, which are very independent in these RAs.
743

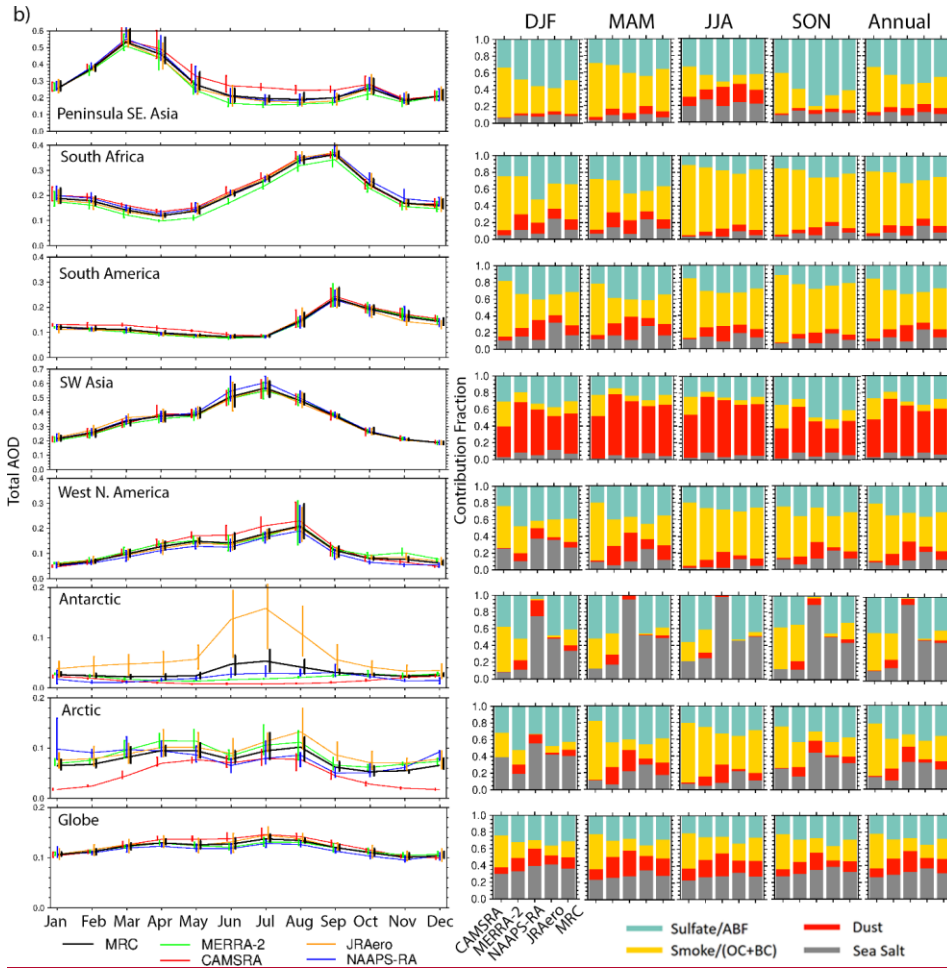




746
747
748
749



750

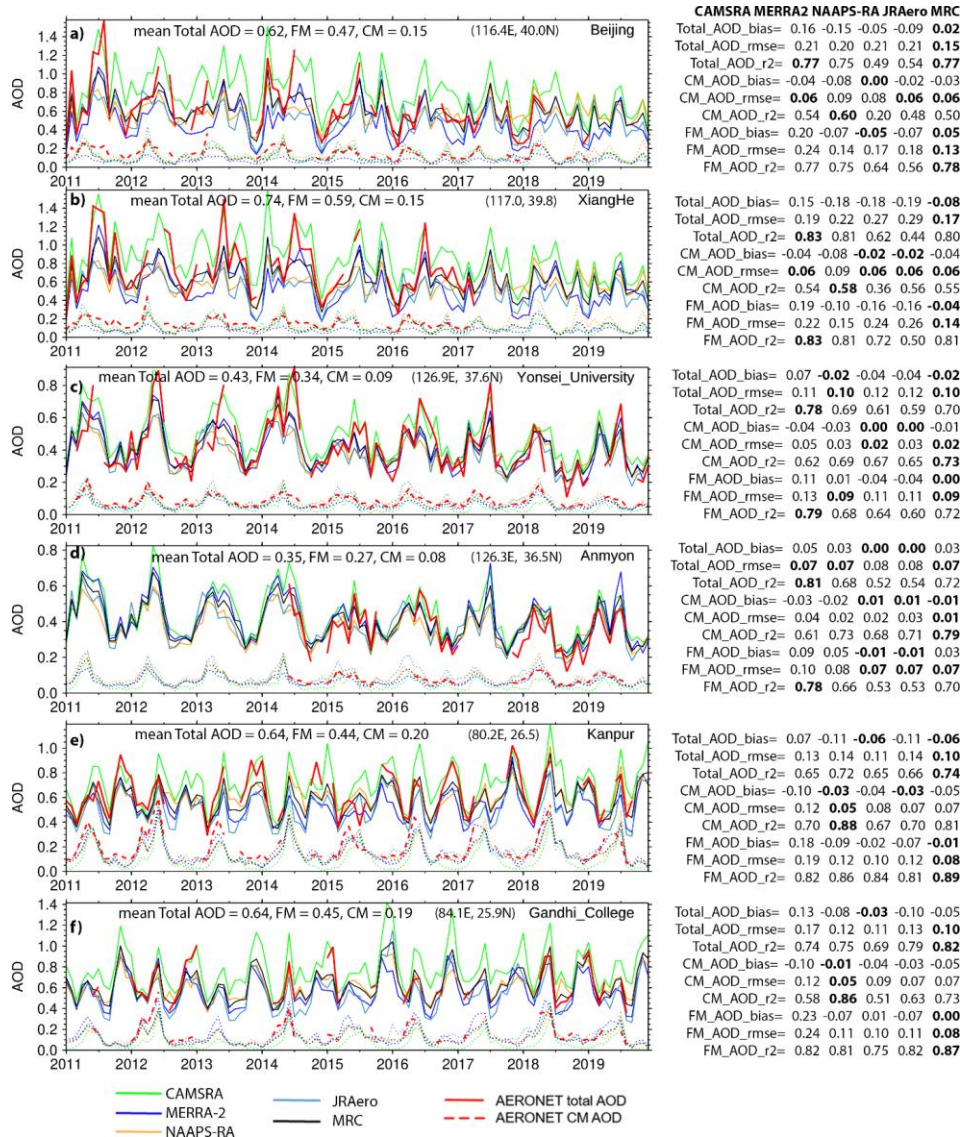


751
 752 Figure 10. Climatological seasonal cycle of regional mean total AOD (left), and the contribution
 753 fraction of speciated AOD to the total AOD for the corresponding regions and seasons from the
 754 four RAs and the MRC (right). Bars in the seasonal cycle plots represent bars denote the
 755 interquartile range of monthly-mean AOD, illustrating interannual variabilities for the period
 756 2011-2019.

757 3.5 Urban versus Rural areas

758 To evaluate the RAs for urban versus rural areas, three paired sites were selected. Beijing
 759 (China), Yonsei University (South Korea) and Kanpur (India) represent urban areas, while their
 760 corresponding rural areas are represented by the Xiang He, Anmyon and Gandhi College sites
 761 among the available AERONET sites. Fig. 11 shows the monthly time series of modal AODs
 762 from the RAs and the MRC, along with their validation statistics against AERONET data. The
 763

764 dominant aerosol mode is FM at all these sites, due mostly to pollution. These sites are also
765 subject to the influence of dust storms in springtime, which contributes to CM AOD. The modal
766 AODs from the four RAs and the MRC generally follow these of AERONET seasonally. The
767 spread among the RAs is relatively large for the Chinese and Indian sites. The spread is relative
768 small for the Korean sites, with the spread being slightly less for the rural site Anmyon than for
769 its corresponding urban site Yonsei University. Regarding bias, RMSE, and r^2 , there is no
770 significant difference between the urban and the corresponding rural sites for each RA and the
771 MRC, despite that r^2 of total AOD tending to be higher for the rural sites than the urban sites.
772 The r^2 of FM AOD also tends to be higher than that of the CM. The RAs and the MRC also
773 capture the decreasing AOD trend in the latter half of the 2011-2019 time period for the Chinese
774 and Korean sites. A more detailed trend analysis will be provided in a companion paper. For the
775 ranking of all RAs in terms of bias, RMSE and r^2 , each individual RA has a few first rankings.
776 MERRA-2 is especially better compared to other RAs at CM/dust AOD for the Indian sites. But
777 in terms of the number of ranking first, the MRC is the winner for all the sites (at least having 5
778 out of 9 statistical variables ranking first for each site).
779



780
781
782
783
784
785
786

Figure 11. Evaluation of total, FM, and CM monthly AODs from the RAs at urban versus rural AERONET sites. Sites a), c) and e) represent urban locations in China, Korea and India respectively, while sites b), d) and f) denote their corresponding rural sites. Mean Total, FM, and CM AODs from AERONET data are presented in the upper panels of the time series plots for each site. The right column displays verification statistics for the four RAs and the MRC.

787 including bias, RMSE and r^2 . Values in bold indicate the lowest bias or RMSE, or the highest r^2 ,
788 signifying the best ranking among all the RAs.

791 4. Conclusions

792 This study compares the monthly average total, and speciated aerosol optical depths (AODs) from
793 four different aerosol reanalyses (RAs). These include the Copernicus Atmosphere Monitoring
794 Service ReAnalysis (CAMSRA) developed by Copernicus/ECMWF; the Japanese Reanalysis for
795 Aerosol (JRAero) developed at the Japan Meteorological Agency (JMA); the Modern-Era
796 Retrospective Analysis for Research and Applications, version 2 (MERRA-2) developed by
797 NASA; and the Navy Aerosol Analysis and Prediction System reanalysis (NAAPS-RA), version
798 1, developed by the U.S. Naval Research Laboratory. The consensus of the four RAs is also
799 developed for intercomparison. The AODs from these RAs are evaluated with AEROSol Robotic
800 NETwork (AERONET) and the ~~combined~~-MODIS Dark Target/Deep Blue retrievals (Levy et al.,
801 2013; Sayer et al. (2014)) using data from 2011-2019. The following are the conclusions drawn
802 from this study:

- 803 1) Global distribution and magnitude of total AOD demonstrate a high level of similarity
804 among all four RAs. The spread of total AOD among the RAs is small over most regions.
805 Exceptions, where the RAs diverge in total AOD are polar regions and areas affected by
806 specific factors, including that include volcanic outgassing, high ~~terrains~~terrain, and certain
807 desert regions.
- 808 2) The relative spread of speciated AODs is considerably larger than that of total AOD.
809 CAMSRA consistently yields higher values for biomass burning (BB) smoke or Organic
810 ~~Aerosol (OA)~~Matter (OM) AOD in comparison to other RAs. Meanwhile, NAAPS-RA
811 exhibits generally higher dust AOD values. JRAero has comparatively high biased inland
812 sea salt AOD. The ~~diversity~~divergence of speciated AODs in regions remote from aerosol
813 sources is large, implying different efficiencies in removal during long-range transport.
814 This phenomenon results from the fact that data assimilation in these RAs constrains total
815 AOD but not speciated AOD.
- 816 3) The seasonality and interannual variability of total AOD in the 16 regions under study,
817 with the exception of the Antarctic and Arctic, demonstrate a high degree of similarity
818 across the various RAs, and align with the observations. While the dominant species of
819 aerosols are consistent across most regions in all RAs, the relative contributions from
820 individual species can vary significantly.
- 821 4) The accuracy of the RAs, as measured by RMSE, bias, and correlation of the total, fine-
822 mode (FM) and coarse-mode (CM) AODs, (i.e. modal AODs), has been verified with
823 AERONET. It is evident that each RA exhibits its own unique regional strengths.
824 Specifically, CAMSRA performs better in South and Southeast Asia, MERRA-2 excels in
825 African and Arabian Peninsula dust regions, NAAPS-RA shows relatively better
826 performance over Europe and East CONUS, and JRAero performs relatively better over
827 southern North America and the Caribbean. Common challenges to all the RAs often

828 include lack or large uncertainty in local emissions, and/or topographic effects, as well as
829 situations where both FM and CM states are mixed. There is no significant difference in
830 RA's performance for urban versus rural areas, despite that rural areas tend to have slightly
831 higher AOD correlations with observations. RAs show the worst performance in areas
832 impacted by mixed FM and CM aerosols, such as South Asia and East Asia, and areas that
833 experience substantial interannual variability in AOD, for instance, Southeast Asia, and the
834 Maritime Continent. The polar regions present a challenge due to limited observations.

835 5) The Multi-Reanalysis-Consensus (MRC), based on an ensemble mean of the four RAs, is
836 not consistently the best performer in terms of RMSE, bias and correlation of modal AODs
837 for a given site or region. However, the MRC generally performs relatively well and
838 remains stable, ranking first or second regionally and first globally among all the RAs,
839 especially for correlation and RMSE. The MRC ranking with respect to correlations is
840 superior to RMSE and then absolute bias. The MRC ranking for CM AOD is slightly
841 superior to that of total AOD and then FM AOD. The MRC method gains an advantage
842 due to its ability to average independent models.

843 The findings presented in this study offer a comprehensive overview of the current state-of-the-art
844 aerosol reanalysesRAs in the context of monthly AOD. The strengths and weaknesses of individual
845 reanalysesRAs and their collective implications will provide valuable information for diverse
846 potential users. Compared to intercomparisons of satellite AOD products, which have shown a
847 typical bias of 15%-25% (which regionally can reach $\pm 50\%$) and AOD diversitydivergence of 10%
848 over ocean to 100% over certain land areas amongst 14 satellite products (in Schutgens et al.,
849 2020), and the intercomparisons of different MODIS products shown in Fig. 1, the biases and
850 diversitydivergence of AODs from the four reanalysesRAs are moderate. The MRC product,
851 which is currently a simple ensemble mean of the four RAs, could be potentially improved with
852 regionally-weighted member contributions according to the strengths of the RAs or with aerosol
853 scenario/species-weighted member contributions.

854 The results of the intercomparison highlight areas for improvement in the next generation of
855 aerosol reanalysesRAs. These improvements may include tuning of emission sources and sinks,
856 finer spatiotemporal resolutions, incorporation of additional aerosol species, such as nitrate
857 aerosols and dust with different mineralogy, separation of BC and OC from BB emissions in some
858 RAs, and application and enhancement of BB plume rise models. Moreover, some centers are
859 planning to incorporate new observational data, such as OMI Aerosol Index to constrain the
860 amount of absorptive aerosols, which has the potential to enhance simulations of BB smoke and
861 dust aerosols (Zhang et al., 2021, Sorenson et al., 2023); Sorenson et al., 2023). Vertical profiles
862 of aerosol backscatter measured by CALIOP and future space-borne lidars may also be
863 incorporated into RAs to help constrain aerosol vertical distribution. Anticipated advancements in
864 emission inventories, retrieval algorithms, space-borne sensors, upcoming satellite missions, and
865 improvements in meteorological and aerosol modelling are expected to drive progress in aerosol
866 reanalysesRA.

867

868

869 **Appendix A: Abbreviations:**

- 870 ABF: Anthropogenic and Biogenic Fine aerosols
871 AERONET: Aerosol Robotic Network
872 AOD: Aerosol Optical Depth
873 AVHRR: Advanced Very High Resolution Radiometer
874 BB: Biomass Burning
875 BC: Black Carbon
876 CALIOP: Cloud-Aerosol Lidar with Orthogonal Polarization (CALIOP)
877 CAMSRA: Copernicus Atmosphere Monitoring System Reanalysis
878 CM: Coarse Mode
879 FLAMBE: Fire Locating and Modeling of Burning Emissions
880 FM: Fine Mode
881 ICAP: International Cooperative for Aerosol Predictions
882 JRAero: the Japanese Reanalysis for Aerosol
883 MASINGAR: Model of Aerosol Species IN the Global Atmosphere
884 MISR: Multi-angle Imaging Spectroradiometer
885 MME: Multi-Model-Ensemble
886 MODIS: Moderate Resolution Imaging Spectroradiometer
887 MODIS-DT: MODIS Dark Target
888 MODIS-DB: MODIS Deep Blue
889 MODIS-DA: MODIS data assimilation quality data.
890 MRC: Multi-reanalysis-consensus
891 NAAPS-RA v1: Naval Aerosol Analysis and Prediction System-Reanalysis version 1.
892 MERRA-2 :Modern-Era Retrospective Analysis for Research and Applications version 2
893 OM: Organic Matter
894 OC: Organic Carbon
895 OMI: Ozone Monitoring Instrument (OMI)
896 PMAp: Polar Multi-Sensor Aerosol product
897 QFED: Quick Fire Emissions Dataset
898 RA: ReAnalysis
899 RMSE: Root Mean Square Error
900 SDA: Spectral Deconvolution Method

901 **Appendix B: Definition of terminologies**

902 Root Mean Square Error (RMSE):

903
$$RMSE = \sqrt{\frac{1}{n} \sum_{i=1}^n (\tau_{model} - \tau_{obs})_i^2}$$
 where τ represents monthly AOD, and n is the total number

904 (i.e. month) of observational or model data.

905 Bias: $\tau_{model} - \tau_{obs}$

906 Mean error: $\frac{1}{n} \sum_{i=1}^n (\tau_{model} - \tau_{obs})_i$

907 Mean absolute error: $\frac{1}{n} \sum_{i=1}^n |\tau_{model} - \tau_{obs}|_i$

908 Coefficient of determination: $r^2 = \frac{(\sum_{i=1}^n (x_i - \bar{x})(y_i - \bar{y}))^2}{\sum_{i=1}^n (x_i - \bar{x})^2 \sum_{i=1}^n (y_i - \bar{y})^2}$

909 where \bar{x} and \bar{y} are the mean values of variable x and y .

910 Multi-Reanalysis-Consensus (MRC): $\frac{1}{m} \sum_{i=1}^m x_i$ where m is the total number of the individual
911 reanalysis, which is 4 for this study.

912 Spread among the RAs is defined as the standard deviation of all the individual models, ie.,

913 $\sigma = \sqrt{\frac{1}{m} \sum_{i=1}^m (x_i - \bar{x})^2}$ where x_i is individual reanalysis, and \bar{x} is the MRC.

914 **Data Availability**

915 All the data supporting the findings of this manuscript can be accessed via the provided links or
916 by requesting them using the contact information provided within those links.

917 AERONET Version 3 Level 2 data: <http://aeronet.gsfc.nasa.gov>

918 MODIS data-assimilation-quality AOD:

919 <https://modaps.modaps.eosdis.nasa.gov/services/about/products/c61-nrt/MCDAODHD.html>

920 CAMSRA AOD: <https://www.ecmwf.int/en/research/climate-reanalysis/cams-reanalysis>

921 JRAero product: <https://www.riam.kyushu-u.ac.jp/taikai/JRAero/>

922 MERRA-2 AOD:

923 [https://disc.gsfc.nasa.gov/datasets/M2TMNXAER_V5.12.4/summary?keywords=%22MERRA-](https://disc.gsfc.nasa.gov/datasets/M2TMNXAER_V5.12.4/summary?keywords=%22MERRA-2%22)
924 [2%22](https://disc.gsfc.nasa.gov/datasets/M2TMNXAER_V5.12.4/summary?keywords=%22MERRA-2%22)

925 NAAPS-RA AOD: [https://usgodae.org/cgi-](https://usgodae.org/cgi-bin/datalist.pl?dset=nrl_naaps_reanalysis&summary=Go)

926 [bin/datalist.pl?dset=nrl_naaps_reanalysis&summary=Go](https://usgodae.org/cgi-bin/datalist.pl?dset=nrl_naaps_reanalysis&summary=Go)

927 MRC AOD: [https://nrlgodae1.nrlmry.navy.mil/cgi-](https://nrlgodae1.nrlmry.navy.mil/cgi-bin/datalist.pl?dset=nrl_mre4_post&summary=Go)

928 [bin/datalist.pl?dset=nrl_mre4_post&summary=Go](https://nrlgodae1.nrlmry.navy.mil/cgi-bin/datalist.pl?dset=nrl_mre4_post&summary=Go)

929

930 **Supplement**

931

932 **Author contributions**

933 PX and JSR designed the study. PX performed the data analysis and wrote the paper with
934 contributions from MA, PRC, KY, TFE, EJH, and JZ on data descriptions [and information](#)
935 [collection](#). All authors contributed to the discussion of the results and revising the paper.

936 **Competing interests**

937 The contact author has declared that none of the authors has any competing interests.

938 **Acknowledgments**

939 The authors acknowledge financial supports from the Office of Naval Research Code 322. Partial
940 support comes from NASA's Interdisciplinary Science (IDS) program (grant no.
941 80NSSC20K1260). We also thank the NASA AERONET and MODIS teams for the AOD data
942 used in the study. We extend our gratitude to NASA GMAO, ECMWF, JMA, U.S. ONR and NRL
943 for providing access to the aerosol reanalysis products.

944 **References**

945 Atwood, S. A., Reid, J. S., Kreidenweis, S. M., Blake, D. R., Jonsson, H. H., Lagrosas, N. D.,
946 Xian, P., Reid, E. A., Sessions, W. R., and Simpas, J. B.: Size-resolved aerosol and cloud
947 condensation nuclei (CCN) properties in the remote marine South China Sea – Part 1:
948 Observations and source classification, *Atmos. Chem. Phys.*, 17, 1105–1123,
949 <https://doi.org/10.5194/acp-17-1105-2017>, 2017.

950 Buchard, V., Silva, A. M. da, Colarco, P. R., Darmenov, A., Randles, C. A., Govindaraju, R.,
951 Torres, O., Campbell, J., and Spurr, R. (2015) Using the OMI aerosol index and absorption
952 aerosol optical depth to evaluate the NASA MERRA Aerosol Reanalysis, *Atmos Chem Phys*, 15,
953 5743–5760, <https://doi.org/10.5194/acp-15-5743-2015>.

954 Buchard, V., Randles, C. A., Silva, A. M. da, Darmenov, A., Colarco, P. R., Govindaraju, R.,
955 Ferrare, R., Hair, J., Beyersdorf, A. J., Ziemba, L. D., and Yu, H. (2017) The MERRA-2 Aerosol
957 Reanalysis, 1980 Onward. Part II: Evaluation and Case Studies, *J Climate*,
958 <https://doi.org/10.1175/jcli-d-16-0613.1>.

959 Colarco, P. R., Kahn, R. A., Remer, L. A., and Levy, R. C. : Impact of satellite viewing-swath
961 width on global and regional aerosol optical thickness statistics and trends. *Atmospheric*
962 *Measurement Techniques*, 7, 2313–2335, 2014.

963 Cui, C.; Liu, Y.; Chen, L.; Liang, S.; Shan, M.; Zhao, J.; Liu, Y.; Yu, S.; Sun, Y.; Mao, J.;
964 Zhang, H.; Gao, S.; Zhenxing Ma, Z (2022) Assessing public health and economic loss
965 associated with black carbon exposure using monitoring and MERRA-2 data, *Environmental*
966 *Pollution*. 313,120190, ISSN 0269-7491, doi: <https://doi.org/10.1016/j.envpol.2022.120190>.

967 Dee, D. P., and A. M. da Silva (1999) Maximum-likelihood estimation of forecast and
968 observation error covariance parameters. Part I: Methodology. *Mon. Wea. Rev.*, 127, 1811–
969 1834, doi:10.1175/1520-0493(1999)127,1822:MLEOFA.2.0.CO;2.

970

971 Dee, D., L. Rukhovets, R. Todling, A. M. da Silva, and J. W. Lawson (2001) An adaptive buddy
972 check for observational quality control. *Quart. J. Roy. Meteor. Soc.*, 127, 2451–2471,
973 doi:10.1002/qj.49712757714.
974
975 Diehl, T., A. Heil, M. Chin, X. Pan, D. Streets, M. Schultz, and S. Kinne (2012) Anthropogenic,
976 biomass burning, and volcanic emissions of black carbon, organic carbon, and SO₂ from 1980 to
977 2010 for hindcast model experiments. *Atmos. Chem. Phys. Discuss.*, 12, 24 895–24 954,
978 doi:10.5194/acpd-12-24895-2012.
979
980 Eck, T.F., Holben, B.N., Reid, J.S., Dubovik, O., Smirnov, A., O’Neill, N.T., Slutsker, I., Kinne,
981 S., 1999. Wavelength dependence of the optical depth of biomass burning, urban, and desert dust
982 aerosols. *J. Geophys. Res.* 104 (D24), 31,333–31,349.
983
984 Eck, T. F., Holben, B. N., Reid, J. S., Xian, P., Giles, D. M., Sinyuk, A., et al.
985 (2018). Observations of the interaction and transport of fine mode aerosols with cloud and/or
986 fog in Northeast Asia from Aerosol Robotic Network and satellite remote sensing. *Journal of*
Geophysical Research: Atmospheres, 123, 5560–5587. <https://doi.org/10.1029/2018JD028313>
987
988 Edwards, E.-L., Reid, J. S., Xian, P., Burton, S. P., Cook, A. L., Crosbie, E. C., Fenn, M. A.,
989 Ferrare, R. A., Freeman, S. W., Hair, J. W., Harper, D. B., Hostetler, C. A., Robinson, C. E.,
990 Scarino, A. J., Shook, M. A., Sokolowsky, G. A., van den Heever, S. C., Winstead, E. L.,
991 Woods, S., Ziemba, L. D., and Sorooshian, A.: Assessment of NAAPS-RA performance in
992 Maritime Southeast Asia during CAMP²Ex, *Atmos. Chem. Phys.*, 22, 12961–12983,
993 <https://doi.org/10.5194/acp-22-12961-2022>, 2022.
994
995 Flemming, J., Benedetti, A., Inness, A., Engelen, R. J., Jones, L., Huijnen, V., Remy, S.,
996 Parrington, M., Suttie, M., Bozzo, A., Peuch, V.-H., Akritidis, D., and Katragkou, E.: The
997 CAMS interim Reanalysis of Carbon Monoxide, Ozone and Aerosol for 2003–2015, *Atmos.*
998 *Chem. Phys.*, 17, 1945–1983, <https://doi.org/10.5194/acp-17-1945-2017>, 2017.
999
1000 Gelaro, R., McCarty, W., Suarez, M. J., Todling, R., Molod, A., Takacs, L., Randles, C. A.,
1001 Darmenov, A., Bosilovich, M. G., Reichle, R., Wargan, K., Coy, L., Cullather, R., Draper, C.,
1002 Akella, S., Buchard, V., Conaty, A., Silva, A. M. da, Gu, W., Kim, G.-K., Koster, R., Lucchesi,
1003 R., Merkova, D., Nielsen, J. E., Partyka, G., Pawson, S., Putman, W., Rienecker, M., Schubert,
1004 S. D., Sienkiewicz, M., and Zhao, B.: The Modern-Era Retrospective Analysis for Research and
1005 Applications, Version 2 (MERRA-2), *J Climate*, 30, 5419–5454, <https://doi.org/10.1175/jcli-d-16-0758.1>, 2017.
1006
1007 Giles, D. M., Sinyuk, A., Sorokin, M. G., Schafer, J. S., Smirnov, A., Slutsker, I., Eck, T. F.,
1008 Holben, B. N., Lewis, J. R., Campbell, J. R., Welton, E. J., Korkin, S. V., and Lyapustin, A. I.:
1009 Advancements in the Aerosol Robotic Network (AERONET) Version 3 database – automated
1010 near-real-time quality control algorithm with improved cloud screening for Sun photometer
1011 aerosol optical depth (AOD) measurements, *Atmos. Meas. Tech.*, 12, 169–
1012 209, <https://doi.org/10.5194/amt-12-169-2019>, 2019.
1013

1014 Ginoux, Paul, M Chin, I Tegen, J M Prospero, B Holben, O Dubovik, and Shian-Jiann Lin:
1015 Sources and distributions of dust aerosols simulated with the GOCART model. *J. Geophys. Res.*,
1016 106(D17), 20255-20273, 2001.

1017 Gliß, J., A. Mortier, M. Schulz, E. Andrews, Y. Balkanski, S.E. Bauer, A.M.K. Benedictow, H.
1018 Bian, R. Checa-Garcia, M. Chin, P. Ginoux, J.J. Griesfeller, A. Heckel, Z. Kipling, A. Kirkevåg,
1019 H. Kokkola, P. Laj, P. Le Sager, M.T. Lund, C. Lund Myhre, H. Matsui, G. Myhre, D. Neubauer,
1020 T. van Noije, P. North, D.J.L. Olivie, L. Sogacheva, T. Takemura, K. Tsigaridis, and S.G. Tsyro,
1021 2021: AeroCom phase III multi-model evaluation of the aerosol life cycle and optical properties
1022 using ground- and space-based remote sensing as well as surface in situ observations. *Atmos.*
1023 *Chem. Phys.*, **21**, no. 1, 87-128, doi:10.5194/acp-21-87-2021.

1024 Gong, S. (2003) A parameterization of sea-salt aerosol source function for sub- and super-micron
1025 particles, *Global Biogeochem Cy*, 17, 1097, <https://doi.org/10.1029/2003gb002079>.

1026 Granier, C., Bessagnet, B., Bond, T., D'Angiola, A., van der Gon, H. D., Frost, G. J., Heil, A.,
1027 Kaiser, J. W., Kinne, S., Klimont, Z., Kloster, S., Lamarque, J.-F., Lioussé, C., Masui, T.,
1028 Meleux, F., Mieville, A., Ohara, T., Raut, J.-C., Riahi, K., Schultz, M. G., Smith, S. J.,
1029 Thompson, A., van Aardenne, J., van der Werf, G. R., and van Vuuren, D. P.: Evolution of
1030 anthropogenic and biomass burning emissions of air pollutants at global and regional scales
1031 during the 1980–2010 period, *Climate Change*, 109, 163–190, 2011. ~~Grzegorski M, Poli G,
1032 Cacciari A, Jafariserajehlou S, Holdak A, Lang R, Vazquez Navarro M, Munro R, Fougnie B.
1033 Multi-Sensor Retrieval of Aerosol Optical Properties for Near-Real-Time Applications Using the
1034 Metop Series of Satellites: Concept, Detailed Description, and First Validation. *Remote Sensing*.
1035 2022; 14(1):85. <https://doi.org/10.3390/rs14010085>.~~

1036 Gumber, A., Reid, J. S., Holz, R. E., Eck, T. F., Hsu, N. C., Levy, R. C., Zhang, J., and Veglio,
1037 P.: Assessment of Severe Aerosol Events from NASA MODIS and VIIRS Aerosol Products for
1038 Data Assimilation and Climate Continuity, *Atmos. Meas. Tech. Discuss.* [preprint],
1039 <https://doi.org/10.5194/amt-2022-290>, in review, 2022

1040 Hogan, T.F. and T.E. Rosmond: The description of the Navy Operational Global Atmospheric
1041 Prediction System's spectral forecast model. *Mon. Wea. Rev.*, 119, 1786-1815, 1991.

1042 Hogan, T. F., Liu, M., Ridout, J. S., Peng, M. S., Whitcomb, T. R., Ruston, B. C., Reynolds, C.
1043 A., Eckermann S. D., Moskaitis, J. R., Baker, N. L., McCormack, J. P., Viner, K. C., McLay, J.
1044 G., Flatau, M. K., Xu, L., Chen, C., and Chang, S. W.: The Navy Global Environmental Model.
1045 *Oceanography*, Special Issue on Navy Operational Models, 27, No. 3. 2014.

1046 Holben, B. N., Eck, T. F., Slutsker, I., Tanre, D., Buis, J. P., Setzer, A., Vermote, E., Reagan, J.
1047 A., Kaufman, Y. J., Nakajima, T., Lavenu, F., Jankowiak, I., and Smirnov, A.: AERONET – A
1048 federated instrument network and data archive for aerosol characterization, *Remote Sens.*
1049 *Environ.*, 66, 1–16, 1998.

Formatted: Font color: Auto, Pattern: Clear

1050 Hsu, N. C., Jeong, M.-J., Bettenhausen, C., Sayer, A. M., Hansell, R., Seftor, C. S., Huang, J.,
1051 and Tsay, S.-C. (2013). Enhanced Deep Blue aerosol retrieval algorithm: The second
1052 generation, *J. Geophys. Res. Atmos.*, 118, 9296–9315, doi:[10.1002/jgrd.50712](https://doi.org/10.1002/jgrd.50712).

1053 Hyer, E. J., Reid, J. S., and Zhang, J.: An over-land aerosol optical depth data set for data
1054 assimilation by filtering, correction, and aggregation of MODIS Collection 5 optical depth
1055 retrievals, *Atmos. Meas. Tech.*, 4, 379–408, <https://doi.org/10.5194/amt-4-379-2011>, 2011.

1056 Ignatov, A., & Stowe, L. (2002). Aerosol Retrievals from Individual AVHRR Channels. Part I:
1057 Retrieval Algorithm and Transition from Dave to 6S Radiative Transfer Model, *Journal of the*
1058 *Atmospheric Sciences*, 59(3), 313-334. Doi: [https://doi.org/10.1175/1520-](https://doi.org/10.1175/1520-0469(2002)059<0313:ARFIAC>2.0.CO;2)
1059 [0469\(2002\)059<0313:ARFIAC>2.0.CO;2](https://doi.org/10.1175/1520-0469(2002)059<0313:ARFIAC>2.0.CO;2)

1060 Inness, A., Ades, M., Agustí-Panareda, A., Barré, J., Benedictow, A., Blechschmidt, A.-M.,
1061 Dominguez, J. J., Engelen, R., Eskes, H., Flemming, J., Huijnen, V., Jones, L., Kipling, Z.,
1062 Massart, S., Parrington, M., Peuch, V.-H., Razinger, M., Remy, S., Schulz, M., and Suttie, M.:
1063 The CAMS reanalysis of atmospheric composition, *Atmos. Chem. Phys.*, 19, 3515–3556,
1064 <https://doi.org/10.5194/acp-19-3515-2019>, 2019.

1065 Kahn, R. A., Gaitley, B. J., Garay, M. J., Diner, D. J., Eck, T. F., Smirnov, A., and Holben, B.
1066 N. (2010), Multiangle Imaging SpectroRadiometer global aerosol product assessment by
1067 comparison with the Aerosol Robotic Network, *J. Geophys. Res.*, 115, D23209,
1068 doi:[10.1029/2010JD014601](https://doi.org/10.1029/2010JD014601).

1069 Kaiser, J. W., Heil, A., Andreae, M. O., Benedetti, A., Chubarova, N., Jones, L., Morcrette, J.-J.,
1070 Razinger, M., Schultz, M. G., Suttie, M., and van der Werf, G. R.: Biomass burning emis-
1071 sions estimated with a global fire assimilation system based on observed fire radiative power,
1072 *Biogeosciences*, 9, 527–554, <https://doi.org/10.5194/bg-9-527-2012>, 2012.

1073 Kinne, S., Schulz, M., Textor, C., Guibert, S., Balkanski, Y., Bauer, S. E., Berntsen, T., Berglen,
1074 T. F., Boucher, O., Chin, M., Collins, W., Dentener, F., Diehl, T., Easter, R., Feichter, J.,
1075 Fillmore, D., Ghan, S., Ginoux, P., Gong, S., Grini, A., Hendricks, J., Herzog, M., Horowitz, L.,
1076 Isaksen, I., Iversen, T., Kirkevåg, A., Kloster, S., Koch, D., Kristjansson, J. E., Krol, M., Lauer,
1077 A., Lamarque, J. F., Lesins, G., Liu, X., Lohmann, U., Montanaro, V., Myhre, G., Penner, J.,
1078 Pitari, G., Reddy, S., Seland, O., Stier, P., Takemura, T., and Tie, X.: An AeroCom initial
1079 assessment – optical properties in aerosol component modules of global models, *Atmos. Chem.*
1080 *Phys.*, 6, 1815–1834, <https://doi.org/10.5194/acp-6-1815-2006>, 2006.
1081

1082 Kramer, S. J., Alvarez, C., Barkley, A. E., Colarco, P. R., Custals, L., Delgado, R., Gaston, C.
1083 J., Govindaraju, R., and Zuidema, P.: Apparent dust size discrepancy in aerosol reanalysis in
1084 north African dust after long-range transport, *Atmos. Chem. Phys.*, 20, 10047–10062,
1085 <https://doi.org/10.5194/acp-20-10047-2020>, 2020.
1086

1087 Jaegle, L., Quinn, P. K., Bates, T. S., Alexander, B., and Lin, J.-T., (2011) Global distribution of
1088 sea salt aerosols: new constraints from in situ and remote sensing observations, *Atmos Chem*
1089 *Phys*, 11, 3137–3157, <https://doi.org/10.5194/acp-11-3137-2011>.

1090 Jenwitheesuk, K.; Peansukwech, U.; Jenwitheesuk, K., (2022) Predictive MERRA-2 aerosol
1091 diagnostic model for oral, oropharyngeal and laryngeal cancer caused by air pollution in Thai
1092 population, *Toxicology Reports*, 9, 970-978. Doi: <https://doi.org/10.1016/j.toxrep.2022.04.015>.
1093

1094 Lacima, A., Petetin, H., Soret, A., Bowdalo, D., Jorba, O., Chen, Z., Méndez Turrubiates, R. F.,
1095 Achebak, H., Ballester, J., and Pérez García-Pando, C.: Long-term evaluation of surface air
1096 pollution in CAMSRA and MERRA-2 global reanalyses over Europe (2003–2020), *Geosci.*
1097 *Model Dev. Discuss.* [preprint], <https://doi.org/10.5194/gmd-2022-197>, in review, 2022.
1098

1099 Levy, R. C.; Mattoo, S.; Munchak, L. A.; Remer, L. A.; Sayer, A. M.; Patadia, F.; Hsu, N. C.
1100 The Collection 6 MODIS aerosol products over land and ocean, *Atmos. Meas. Tech.*, 2013, 6,
1101 2989-3034, <https://doi.org/10.5194/amt-6-2989-2013>.
1102

1103 Lynch, P., Reid, J. S., Westphal, D. L., Zhang, J., Hogan, T. F., Hyer, E. J., Curtis, C. A., Hegg,
1104 D. A., Shi, Y., Campbell, J. R., Rubin, J. I., Sessions, W. R., Turk, F. J., and Walker, A. L.: An
1105 11-year global gridded aerosol optical thickness reanalysis (v1.0) for atmospheric and climate
1106 sciences, *Geosci. Model Dev.*, 9, 1489–1522, <https://doi.org/10.5194/gmd-9-1489-2016>, 2016.

1107 McCoy, D. T., F. A.-M. Bender, J. K. C. Mohrmann, D. L. Hartmann, R. Wood, and D. P.
1108 Grosvenor (2017): The global aerosol-cloud first indirect effect estimated using MODIS,
1109 MERRA, and AeroCom, *J. Geophys. Res. Atmos.*, 122, 1779–1796, doi:10.1002/2016JD026141.

1110 Monahan, E. C., Spiel, D. E., and Davidson, K. L.: A model of marine aerosol generation via
1111 whitecaps and wave disruption, in *Oceanic Whitecaps*, edited by: Monahan, E. and Niocaill, G.
1112 M., D. Reidel, Norwell, Mass., 167–174, 1986.

1113 Ningombam, Shantikumar S., Dumka, Umesh Chandra, Mugil, Sivasamy Kalamani, Kuniyal,
1114 Jagdish Chandra, Hooda, Rakesh K., Gautam, Alok Sagar, and Tiwari, Suresh, 2021, "Impacts of
1115 Aerosol Loading in the Hindu Kush Himalayan Region Based on MERRA-2 Reanalysis Data"
1116 *Atmosphere* Vol. 12, No. 10, pp 1290, 2073-4433

1117 Ohno, T., Irie, H., Momoi, M. and da Silva, A.M. : Quantitative evaluation of mixed biomass
1118 burning and anthropogenic aerosols over the Indochina Peninsula using MERRA-2 reanalysis
1119 products validated by sky radiometer and MAX-DOAS observations. *Prog Earth Planet Sci* 9, 61
1120 (2022). <https://doi.org/10.1186/s40645-022-00520-4>

1121

1122 O'Neill, N.T., Eck, T. F., Holben, B. N., Smirnov, A., Dubovik, O. and Royer, A.: Bimodal size
1123 distribution influences on the variation of Angstrom derivatives in spectral and optical depth
1124 space, *J. Geophys. Res.*, 106, 9787-9806, 2001.
1125

1126 O'Neill, N. T., Eck, T. F., Smirnov, A., Holben, B. N., and Thulasiraman, S.: Spectral
1127 discrimination of coarse and fine mode optical depth. *J. Geophys. Res.*, 108, D05212,
1128 doi:10.1029/2002JD002975, 2003.
1129

1130 O'Sullivan, D., Marengo, F., Ryder, C. L., Pradhan, Y., Kipling, Z., Johnson, B., Benedetti, A.,
1131 Brooks, M., McGill, M., Yorks, J., and Selmer, P.: Models transport Saharan dust too low in the

1132 atmosphere: a comparison of the MetUM and CAMS forecasts with observations, *Atmos. Chem.*
1133 *Phys.*, 20, 12955–12982, <https://doi.org/10.5194/acp-20-12955-2020>, 2020.

1134

1135 [Popp, T., deLeeuw, G., Bingen, C., Brühl, C., Capelle, V., Chedin, A., Clarisse, L., Dubovik, O.,](#)
1136 [Grainger, R., Griesfeller, J., Heckel, A., Kinne, S., Klüser, L., Kosmale, M., Kolmonen, P.,](#)
1137 [Lelli, L., Litvinov, P., Mei, L., North, P., Pinnock, S., Povey, A., Robert, C., Schulz, M.,](#)
1138 [Sogacheva, L., Stebel, K., Zweers, D. S., Thomas, G., Gijssbert Tilstra, L., Vandenbussche, S.,](#)
1139 [Veefkind, P., Vountas, M., and Xue, Y.: Development, production and evaluation of aerosol](#)
1140 [climate data records from european satellite observations \(Aerosol_cci\), *Remote Sensing*, 8,](#)
1141 [421, <https://doi.org/10.3390/rs8050421>, 2016.](#)

1142 Randles, C. A., daSilva, A. M., Buchard, V., Colarco, P. R., Darmenov, A., Govindaraju, R., et
1143 al.: The MERRA-2 aerosol reanalysis, 1980 onward. Part I: System description and data
1144 assimilation evaluation. *Journal of Climate*, 30(17), 6823–6850. [https://doi.org/10.1175/JCLI-D-](https://doi.org/10.1175/JCLI-D-16-0609.1)
1145 [16-0609.1](#), 2017.

1146 Reid, J.S., Gumber, A.; Zhang, J.; Holz, R. E.; Rubin, J. I.; Xian, P.; Smirnov, A.; Eck, T. F.;
1147 O’Neill, N. T.; Levy, R. C.; Reid, E. A.; Colarco, P. R.; Benedetti, A.; and Tanaka, T. (2022) A
1148 Coupled Evaluation of Operational MODIS and Model Aerosol Products for Maritime
1149 Environments Using Sun Photometry: Evaluation of the Fine and Coarse Mode. *Remote Sens*,
1150 14, 2978. <https://doi.org/10.3390/rs14132978>.

1151 Reid, J. S., and Coauthors, 2023: The coupling between tropical meteorology, aerosol lifecycle,
1152 convection, and radiation, during the Cloud, Aerosol and Monsoon Processes Philippines
1153 Experiment (CAMP2Ex). *Bull. Amer. Meteor. Soc.*, E1179–E1205,
1154 <https://doi.org/10.1175/BAMS-D-21-0285.1>

1155 Reid, J. S., Hyer, E. J., Prins, E. M., Westphal, D. L., Zhang, J., Wang, J., Christopher, S. A.,
1156 Curtis, C. A., Schmidt, C. C., Eleuterio, D. P., Richardson, K. A., and Hoffman, J. P.: Global
1157 Monitoring and Forecasting of Biomass-Burning Smoke: Description of and Lessons from the
1158 Fire Locating and Modeling of Burning Emissions (FLAMBE) Program, *IEEE J. Sel. Top.*
1159 *Appl.*, 2, 144–162, JSTARS-2009-00034, 2009.

1160 Reid, J. S., Xian, P., Hyer, E. J., Flatau, M. K., Ramirez, E. M., Turk, F. J., Sampson, C. R.,
1161 Zhang, C., Fukada, E. M., and Maloney, E. D.: Multi-scale meteorological conceptual analysis of
1162 observed active fire hotspot activity and smoke optical depth in the Maritime Continent, *Atmos.*
1163 *Chem. Phys.*, 12, 2117–2147, <https://doi.org/10.5194/acp-12-2117-2012>, 2012.

1164 Reid, J. S., Xian, P., Holben, B. N., Hyer, E. J., Reid, E. A., Salinas, S. V., Zhang, J., Campbell,
1165 J. R., Chew, B. N., Holz, R. E., Kuciauskas, A. P., Lagrosas, N., Posselt, D. J., Sampson, C. R.,
1166 Walker, A. L., Welton, E. J., and Zhang, C.: Aerosol meteorology of the Maritime Continent for
1167 the 2012 7SEAS southwest monsoon intensive study – Part 1: regional-scale phenomena, *Atmos.*
1168 *Chem. Phys.*, 16, 14041–14056, <https://doi.org/10.5194/acp-16-14041-2016>, 2016.

1169 Roychoudhury, C., He, C., Kumar, R., McKinnon, J. M., & Arellano, A. F. Jr. (2022). On the
1170 relevance of aerosols to snow cover variability over High Mountain Asia. *Geophysical Research*
1171 *Letters*, 49, e2022GL099317. <https://doi.org/10.1029/2022GL099317>

1172 Sayer, A.M., Munchak, L.A., Hsu, N.C., Levy, R.C., Bettenhausen, C., Jeong, M.J., 2014.
1173 MODIS Collection 6 aerosol products: comparison between Aqua’s e-Deep Blue, Dark Target,
1174 and “merged” _data sets, and usage recommendations. *J. Geophys. Res. Atmos.* 119 (24), 13–
1175 965.

1176 Schutgens, N., Sayer, A. M., Heckel, A., Hsu, C., Jethva, H., de Leeuw, G., Leonard, P. J. T.,
1177 Levy, R. C., Lipponen, A., Lyapustin, A., North, P., Popp, T., Poulsen, C., Sawyer, V.,
1178 Sogacheva, L., Thomas, G., Torres, O., Wang, Y., Kinne, S., Schulz, M., and Stier, P.: An
1179 AeroCom–AeroSat study: intercomparison of satellite AOD datasets for aerosol model
1180 evaluation, *Atmos. Chem. Phys.*, 20, 12431–12457, <https://doi.org/10.5194/acp-20-12431-2020>,
1181 2020.

1182
1183 [Sessions, W. R., Reid, J. S., Benedetti, A., Colarco, P. R., da Silva, A., Lu, S., Sekiyama, T.,](#)
1184 [Tanaka, T. Y., Baldasano, J. M., Basart, S., Brooks, M. E., Eck, T. F., Iredell, M., Hansen, J. A.,](#)
1185 [Jorba, O. C., Juang, H.-M. H., Lynch, P., Morcrette, J.-J., Moorthi, S., Mulcahy, J., Pradhan, Y.,](#)
1186 [Razinger, M., Sampson, C. B., Wang, J., and Westphal, D. L. \(2015\) Development towards a](#)
1187 [global operational aerosol consensus: basic climatological characteristics of the International](#)
1188 [Cooperative for Aerosol Prediction Multi-Model Ensemble \(ICAP-MME\).](#) *Atmos. Chem. Phys.*
1189 [15, 335-362](#)

1190
1191 Shi, Y., Zhang, J., Reid, J. S., Hyer, E. J., and Hsu, N. C.: Critical evaluation of the MODIS
1192 Deep Blue aerosol optical depth product for data assimilation over North Africa, *Atmos. Meas.*
1193 *Tech.*, 6, 949–969, <https://doi.org/10.5194/amt-6-949-2013>, 2013.

1194
1195 Shi, Y., Zhang, J., Reid, J. S., Holben, B., Hyer, E. J., and Curtis, C.: An analysis of the
1196 collection 5 MODIS over-ocean aerosol optical depth product for its implication in aerosol
1197 assimilation, *Atmos. Chem. Phys.*, 11, 557–565, <https://doi.org/10.5194/acp-11-557-2011>, 2011.
1198

1199 Sorenson, B. T., Zhang, J., Reid, J. S., Xian, P., and Jaker, S. L.: Ozone Monitoring Instrument
1200 (OMI) UV aerosol index data analysis over the Arctic region for future data assimilation and
1201 climate forcing applications, *Atmos. Chem. Phys.*, 23, 7161–7175, <https://doi.org/10.5194/acp-23-7161-2023>, 2023.
1202

1203
1204 Textor, C., Schulz, M., Guibert, S., Kinne, S., Balkanski, Y., Bauer, S., Berntsen, T., Berglen, T.,
1205 Boucher, O., Chin, M., Dentener, F., Diehl, T., Easter, R., Feichter, H., Fillmore, D., Ghan, S.,
1206 Ginoux, P., Gong, S., Grini, A., Hendricks, J., Horowitz, L., Huang, P., Isaksen, I., Iversen, I.,
1207 Kloster, S., Koch, D., Kirkevåg, A., Kristjansson, J. E., Krol, M., Lauer, A., Lamarque, J. F., Liu,
1208 X., Montanaro, V., Myhre, G., Penner, J., Pitari, G., Reddy, S., Seland, Ø., Stier, P., Takemura,
1209 T., and Tie, X.: Analysis and quantification of the diversities of aerosol life cycles within
1210 AeroCom, *Atmos. Chem. Phys.*, 6, 1777–1813, <https://doi.org/10.5194/acp-6-1777-2006>, 2006.
1211

1212 Tong, D. Q., et al., Health and Safety Effects of Airborne Soil Dust in the Americas and Beyond.
1213 *Reviews of Geophysics.* <https://doi.org/10.1029/2021RG000763>

1214
1215 Xian, P., Klotzbach, P. J., Dunion, J. P., Janiga, M. A., Reid, J. S., Colarco, P. R., and Kipling,
1216 Z.: Revisiting the relationship between Atlantic dust and tropical cyclone activity using aerosol
1217 optical depth reanalyses: 2003–2018, *Atmos. Chem. Phys.*, 20, 15357–15378,
1218 <https://doi.org/10.5194/acp-20-15357-2020>, 2020.
1219
1220 Xian, P., Reid J. S., Hyer, E., Sampson, C.R., Rubin, J., Ades M., et. al., Current state of the
1221 global operational aerosol multi-model ensemble: an update from the International Cooperative
1222 for Aerosol Prediction (ICAP), *Quarterly J. of the Royal Met. Soc.*
1223 <https://doi.org/10.1002/qj.3497>, 2019.
1224
1225 Xian, P., Reid, J. S., Turk, J. F., Hyer, E. J., and Westphal, D. L.: Impact of models versus
1226 satellite measured tropical precipitation on regional smoke optical thickness in an aerosol
1227 transport model, *Geophys. Res. Lett.*, 36, L16805, doi:10.1029/2009GL038823, 2009.
1228
1229 Xian, P., Reid, J. S., Atwood, S. A., Johnson, R. S., Hyer, E. J., Westphal, D. L., Sessions, W.:
1230 Smoke aerosol transport patterns over the Maritime continent, *Atmos. Res. Vol. 122*, 469–485,
1231 <https://doi.org/10.1016/j.atmosres.2012.05.006>
1232 Xian, P., Zhang, J., O'Neill, N. T., Toth, T. D., Sorenson, B., Colarco, P. R., Kipling, Z., Hyer, E.
1233 J., Campbell, J. R., Reid, J. S., and Ranjbar, K.: Arctic spring and summertime aerosol optical
1234 depth baseline from long-term observations and model reanalyses – Part 1: Climatology and
1235 trend, *Atmos. Chem. Phys.*, 22, 9915–9947, <https://doi.org/10.5194/acp-22-9915-2022>, 2022.
1236 Witek, M. L., P. J. Flatau, P. K. Quinn, and D. L. Westphal: Global sea-salt modeling: Results
1237 and validation against multicampaign shipboard measurements, *J. Geophys. Res.*, 112, 2007.
1238 Yumimoto, K., Tanaka, T. Y., Oshima, N., and Maki, T.: JRAero: the Japanese Reanalysis for
1239 Aerosol v1.0, *Geosci. Model Dev.*, 10, 3225–3253, <https://doi.org/10.5194/gmd-10-3225-2017>,
1240 2017.
1241 Yukimoto, S., Adachi, Y., Hosaka, M., Sakami, T., Yoshimura, H., Hirabara, M., Tanaka, T. Y.,
1242 Shindo, E., Tsujino, H., Deushi, M., Mizuta, R., Yabu, S., Obata, A., Nakano, H., Koshiro, T.,
1243 Ose, T., and Kitoh, A.: A New Global Climate Model of the Meteorological Research Institute:
1244 MRI-CGCM3 –Model Description and Basic Performance, *J. Meteorol. Soc. Jpn.*, 90A, 23–64,
1245 <https://doi.org/10.2151/jmsj.2012-A02>, 2012.
1246 Zhang, J. L., and J. S. Reid: MODIS aerosol product analysis for data assimilation: Assessment
1247 of over-ocean level 2 aerosol optical thickness retrievals. *J. Geophys. Res.-Atmos.*, 111, 2006.
1248
1249 Zhang, J. L., and Reid, J. S., Westphal, D. L., Baker, N. L., and Hyer, E. J.: A system for
1250 operational aerosol optical depth data assimilation over global oceans. *J. Geophys. Res.*, 113,
1251 D10208, doi:10.1029/2007JD009065, 2008.
1252
1253 Zhang J., Reid, J. S., Alfaro-Contreras, R., Xian P., Has China been exporting less particulate air
1254 pollution over the past decade?, *Geophysical Research Letters*, 10.1002/2017GL072617, 2017.

1255
1256 Zhang, J., Spurr, R. J. D., Reid, J. S., Xian, P., Colarco, P. R., Campbell, J. R., Hyer, E. J., and
1257 Baker, N. L.: Development of an Ozone Monitoring Instrument (OMI) aerosol index (AI) data
1258 assimilation scheme for aerosol modeling over bright surfaces – a step toward direct radiance
1259 assimilation in the UV spectrum, *Geosci. Model Dev.*, 14, 27–42, [https://doi.org/10.5194/gmd-](https://doi.org/10.5194/gmd-14-27-2021)
1260 [14-27-2021](https://doi.org/10.5194/gmd-14-27-2021), 2021.
1261
1262 Zhang, X., and Zhou, Y.: Aerosol direct radiative forcing over China: A 40-year MERRA-2-
1263 based evaluation, *Atmos. Env.*, Vol., 299, <https://doi.org/10.1016/j.atmosenv.2023.119659>